



# Linkage between moisture transport over the Yangtze River Basin and a critical area of the Tibetan Plateau during the Meiyu

Lili Dong<sup>1,2</sup> · Xiangde Xu<sup>2</sup> · Tianliang Zhao<sup>2</sup> · Hongchang Ren<sup>3</sup>

Received: 7 July 2018 / Accepted: 24 January 2019 / Published online: 22 February 2019  
© Springer-Verlag GmbH Germany, part of Springer Nature 2019

## Abstract

Located downstream of the Tibetan Plateau (TP), the Yangtze River Basin (YRB) in China frequently experiences torrential rainfall and severe rainstorms within the zonally elongate Meiyu belt. Inter-annual variations in drought and flooding in the YRB are shown to be highly correlated with the upstream surface latent heat flux (SLHF) over the TP, suggesting that the SLHF over the TP can be a “strong signal” of Meiyu variability. Results show that the southeastern margin of the TP (SEMP) is the most “sensitivity area” of the “strong signal”. On inter-annual scales, low (high) SLHF over the SEMTP corresponds to high (low) humidity at upper levels, strong (weak) zonal moisture transport and a southerly (northerly) pattern of East Asian summer monsoon (EASM) moisture transport circulation in July. The anomalous moisture flow originating from the mid to low latitude oceans, converges in the east of the SEMTP and turns eastward (northward); thus, the SEMTP acts as the key area of redirection of moisture flow. The ridge of moisture transport is located at about 22.5°N (29.5°N) in East China for low (high) SLHF over the SEMTP. Under low SLHF conditions, the warm, humid airflow from the SEMTP creates favorable conditions for Meiyu rainfall and torrential rainstorms. Numerical simulation and sensitivity analyses using the mesoscale Weather Research and Forecasting (WRF) model further reveal that SLHF over the SEMTP shows pronounced “strong signal” features. The variation of intensity of SLHF over the SEMTP corresponds to the moisture transport structure of the Meiyu rain belt and the location of the ridge of the subtropical high in East China. An increase in the apparent heat source Q1 over the main body of the TP might explain the “strong signal” over the SEMTP. This apparent heat source plays an important role in modulating both the SLHF over the SEMTP and the location of the subtropical high circulation system.

**Keywords** “Sensitivity area” of the Tibetan Plateau · Yangtze River Basin · Meiyu · Surface latent heat flux · “Strong signal” · Moisture transport

## 1 Introduction

The Yangtze River Basin (YRB), which covers several hundred thousand square kilometers, is the main industrial and agricultural hub in China and is the most densely populated area of the country. The YRB is located downstream of the

Tibetan Plateau (TP) and experiences an East Asian Monsoon (EAM) climate. It is one of the most flood- and storm-prone areas in the world and is frequently hit by torrential rainfall and severe floods (Ye and Gao 1979; Ding 1992, 2009; Wu and Zhang 1998; Lu et al. 2005; Xu et al. 2008a; Liu et al. 2012; Boos and Kuang 2013); e.g., the torrential rainstorms of 1954 and 1998 brought more than 600 mm precipitation over much of the YRB. The heavy rainfall and disastrous floods in this region often cause significant economic losses. Therefore, finding an upstream “strong signal” of rainstorms over the YRB would be important for national disaster prevention and mitigation.

The TP is the world’s highest plateau and is characterized by complex terrain. It has strong dynamic and thermodynamic impacts on the atmospheric circulation over East Asia (Huang and Yan 1987; Wu and Zhang 1998; Wang et al. 2011; Wang et al. 2018) and the regional distribution of

✉ Xiangde Xu  
xuxd@cma.gov.cn

Lili Dong  
dlldsflsm@foxmail.com

<sup>1</sup> Nanjing University of Information Science and Technology, Nanjing 210044, China

<sup>2</sup> State Key Laboratory of Severe Weather, Chinese Academy of Meteorological Sciences, Beijing 100081, China

<sup>3</sup> National Meteorological Center, China Meteorological Administration, Beijing 100081, China

precipitation (Duan and Xiao 2015; Wang et al. 2015). Simulations have shown that the northern branch of the South Asian summer monsoon cannot form if the platform of the TP is removed, and only the southern Himalayan Mountains are retained in the absence of the surface sensible heat flux from the Himalayan surface (Wu et al. 2012). Wang et al. (2016) used the Weather Research and Forecasting Model (WRF) regional model to show that the slope topographic heating of the Himalayan region in the southern TP plays an important role in regulating the local atmospheric circulation and precipitation, and is a dominant factor in the formation and maintenance of the northern branch of the South Asian summer monsoon. Xu et al. (2008b, 2014) described the TP as the “world’s water tower”, possessing a self-exciting feedback mechanism similar to the CISK (conditional instability of the second kind) mechanism of tropical cyclones.

The World Meteorological Organization (WMO) World Weather Research Program (WWRP)/THORPEX (The Observing-system Research and Predictability Experiment) showed that for high-impact weather systems in a specific target region, there are usually corresponding sensitivity areas upstream. The appropriate assimilation of observations in the upstream sensitivity areas into a numerical model can effectively improve the forecast accuracy in the targeted downstream region. Therefore, for forecasts of high-impact weather, such as heavy rainfall in the YRB, there might exist corresponding upstream sensitivity areas over the TP. Observations in the “sensitivity area” are most effective in improving the forecast accuracy of rainstorms over the YRB. In fact, previous studies have pointed out that the TP constantly attracts a warm and humid airflow from the adjacent Indian Ocean, the South China Sea, and the low-latitude Pacific Ocean through the so-called “heat pump” effect (Wu and Zhang 1998; Xu and Miao 1998; Xu et al. 2002a). This process redistributes the moisture conveyed from the low-latitude oceans, which is the key factor affecting moisture transport in the YRB during the Meiyu period. However, there are few meteorological observation sites on the TP, which gives rise to large uncertainty in weather observations over the TP and downstream regions, especially the YRB.

In 2006–2009, Chinese and Japanese scientists jointly established the Japan International Cooperation Agency (JICA), a new-generation integrated meteorological observation system on the TP and surrounding region (hereafter referred to as the JICA-TP observation system). The key observational region was selected over the TP and its eastern margin. Xu (2009) conducted WRF simulations assimilating automatic weather station (AWS) data from the SEMTP, showing that the assimilation of AWS data over the SEMTP is helpful in revealing the 3-D atmospheric dynamic and thermal structure of severe weather systems on the eastern plateau and identifying the strong signal of their occurrence and development.

Based on the idea of identifying the upstream “sensitivity area” as discussed in THORPEX, it is important to improve our understanding of the generation of heavy rainfall and flooding in the YRB during summer and track the “strong signal” of the remote connection in the upstream “sensitivity area” on the TP. This is a key approach to exploring the development of the Meiyu frontal system and the causes of sustained rainstorms over the YRB, and it is also great value for disaster prevention and mitigation. Therefore, it is necessary to identify the upstream “sensitivity area” for the Meiyu over the YRB and understand the related variation in the Meiyu to the “strong signal” from the upstream “sensitivity area”. These are key issues in both theoretical study and forecasting in terms of understanding the influence of the TP on weather systems.

This study attempts to elucidate the relationship between land-atmosphere processes over the “sensitivity area” and the Meiyu belt in the downstream YRB. The remainder of the manuscript is organized as follows. The datasets and models are described in Sect. 2, and Sect. 3 presents the spatiotemporal characteristics of the Meiyu belt and rainstorm frequency in the YRB. Section 4 traces the upstream “strong signal” over the TP for the Meiyu over the YRB, and Sect. 5 presents the moisture transport of the anomalous precipitation and rainstorm frequency over the YRB and the related SLHF over the “sensitivity area”. Section 6 analyzes the features of the correlation between SLHF over the “sensitivity area” and the moisture transport circulation pattern around the subtropical high in depth. Section 7 analyzes the simulation results, and the conclusions are provided in Sect. 8.

## 2 Data and approach

### 2.1 Data

The data used in this study are as follows: (1) daily precipitation data for the period 1979–2014 from 601 stations from the National Meteorological Center of the China Meteorological Administration (CMA) observation archives. The daily data were transformed to monthly data to analyze the seasonality of Meiyu precipitation over China. Daily precipitation data were used to calculate the days of rainstorm occurrence in each month with daily precipitation  $\geq 50$  mm as the rainstorm criterion, and daily precipitation  $\geq 100$  mm for torrential rainstorms. The 601 ground weather stations cover the entire Chinese mainland and effectively represent the spatiotemporal distribution of rainstorms over mainland China (Xu et al. 2017); (2) low level cloud cover daily data from 753 observational stations in China over 1951–2010 by the CMA; (3) European Centre for Medium-Range Weather Forecasts (ECMWF) ERA-Interim reanalysis monthly mean surface fluxes, together with wind field, air temperature,

specific humidity, and pressure, with a horizontal resolution of  $0.75^\circ \times 0.75^\circ$  and 37 vertical levels extending from 1000 hPa to 1 hPa during 1979–2014 and 6-hourly data for July 1998 for the initial and boundary conditions of the WRF model. (ECMWF, <http://apps.ecmwf.int/datasets/data/interim-full-mnfh/levtype=sfc/>); (4) data from a comprehensive boundary layer observation station established in the SEMTP, at Dali, Yunnan Province ( $25.7^\circ\text{N}$ ,  $100.18^\circ\text{E}$ , altitude 1990.5 m) in 2008 as part of JICA-TP observation system (Xu 2009). This station focuses on observations of ground turbulence and radiation, temperature, humidity, wind profile, soil heat flux, hydrological conditions, and other land–atmosphere processes. These in situ data were used for a comparison with ECMWF reanalysis data from March 5, 2008 to July 6, 2009 and for July 2014–2016; (5) Monthly precipitation data provided by the CMA and the Climate Research Unit (CRU) at the University of East Anglia with a spatial resolution of  $0.5^\circ \times 0.5^\circ$  over the period 1901–2000 (New et al. 2002).

## 2.2 Methods

### 2.2.1 Anomaly index

Statistically, the ratio of anomaly to the standard deviation can be used as an anomaly index to quantify the intensity of extreme weather and climate events. The anomaly index  $K_i$  can be calculated as follows (Zhang and Li 2007):

$$K_i = \frac{(X_i - X)}{S} \quad (1)$$

where  $X_i$  is the value for a year (season, month, or a time interval),  $X$  is the climatological mean of  $X_i$ , and  $S$  is the standard deviation.  $K_i > 1$  indicates data above normal conditions and  $K_i < -1$  indicates data below normal conditions. An absolute value of  $K_i$  between 0 and 1 indicates normal conditions. In this paper, Eq. (1) is used to calculate anomaly indexes of SLHF over the SEMTP and of Meiyu rainfall and rainstorm frequency over the YRB.

### 2.2.2 Moisture transport and correlation vector

To analyze the correlation between SLHF over the SEMTP and the moisture transport flux over the entire atmospheric column (hereafter, the integrated moisture transport flux) and elucidate the impact of the thermal forcing of the TP on the annual moisture transport, the integrated moisture transport flux per unit area is calculated as follows:

$$Q = \frac{1}{g} \int_{p_t}^{p_s} \vec{V} q dp \quad (2)$$

where  $g$  is gravitational acceleration,  $\vec{V}$  is the wind velocity vector at all layers over the unit air column,  $p_s$  is the surface

pressure and  $p_t$  is the air pressure at the atmospheric upper boundary layer (set as 300 hPa here). The components of  $Q$  are  $qu$  and  $qv$ , which are the integrated moisture transport fluxes in the  $u$  (zonal) and  $v$  (meridional) directions respectively. The correlation vector is expressed as

$$\mathbf{R}(x, y) = R_u(x, y)\mathbf{i} + R_v(x, y)\mathbf{j} \quad (3)$$

where  $R_u$  and  $R_v$  are the zonal and meridional components of the correlation vector  $\mathbf{R}$ , respectively (positive  $R_u$  indicates eastward while positive  $R_v$  indicates northward).

### 2.2.3 Calculation of apparent heat source (Q1)

The apparent heat source Q1 is calculated as follows (Yanai 1961; Yanai and Tomita 1998):

$$Q1 = C_p \left( \frac{\partial T}{\partial t} + \vec{V} \cdot \nabla T + \left( \frac{P}{P_0} \right)^k \omega \frac{\partial \theta}{\partial p} \right) \quad (4)$$

where  $Q1$  is the heating rate per unit air mass,  $\kappa = R/C_p$  with the gas constant  $R$ ,  $C_p$  is the specific heat capacity of air at constant pressure, and  $\theta$  is the potential temperature. The three terms on the right-hand side of the equation are the local rate of change, horizontal advection, and vertical advection. Integrating both sides of Eq. (4) from  $p_s$  to  $p_t$ , the apparent heat source over the entire atmospheric column (hereafter, the integrated apparent heat source) is

$$\langle Q1 \rangle = \frac{1}{g} \int_{p_t}^{p_s} Q1 dp. \quad (5)$$

## 2.3 Models

### 2.3.1 FLEXPART Lagrangian particle dispersion model

The Lagrangian particle dispersion model, FLEXPART (FLEXible PARTicle dispersion model), developed at the Norwegian Institute for Air Research (Stohl et al. 2005), is used to calculate spatiotemporal variations in moisture transport trajectories over the SEMTP. FLEXPART calculates the trajectories of many particle swarms, and the trajectories can be used to describe tracer transport and dispersion in the atmosphere. In this paper, FLEXPART was used to calculate the forward trajectories of moisture particles over the SEMTP. The ECMWF reanalysis data were used as the driving field. A particle swarm was initialized over the SEMTP within  $98^\circ\text{--}105^\circ\text{E}$ ,  $23^\circ\text{--}32.5^\circ\text{N}$  and between 100 m and 6000 m height. The calculation period was from 00:00 on July 17, 1998 to 00:00 on July 22, 1998.

### 2.3.2 WRF model and experiment design

Regional models often have higher spatial resolution than global models so that they resolve local- and regional-scale physical and dynamic processes. Hence, a regional model that can better capture the terrain and other land features of the TP is an important tool to advance our understanding of the East Asian regional climate and climate change. Regional climate models have been increasingly used to study the impact of the TP on precipitation over East China (Maussion et al. 2011; Wang et al. 2014a, 2016; Gao et al. 2015; Wu et al. 2016). This paper uses the WRF (Version 3.4.1, Skamarock et al. 2008) as a modeling tool. The model uses the Mercator projection centered at 125°E and 27°N, and the simulation area is configured with two-way nesting. The outer domain covers most of Asia and the Arabian Sea, the Bay of Bengal, and the South China Sea with 27 km spatial resolution. The inner domain (d02) covers the land and sea areas over the TP downstream area (105°–180°E, 22.5°–40°N), with a horizontal resolution of 9 km and 28 vertical layers from the surface to 50 hPa, taken as the upper boundary (Fig. 1). The physical parameterization schemes appropriate for the region based on large numbers of experiments using different combinations of parameterization schemes and experience from previous work (Li 2012; Li et al. 2017a). For example, previous studies have shown that parameterizing the boundary layer with the local turbulent kinetic energy scheme BouLac gives a more realistic EASM than the non-local closure schemes YSU and ACM2. A model with BouLac can better simulate the southwesterly air flow in the middle and lower troposphere, the Western Pacific Subtropical High, and EASM precipitation in East China (Wang et al. 2014b). The WSM6 microphysical process scheme gives the changing location of the subtropical high that is close to observations (Lin et al. 2010). Therefore the following physical parameterization schemes are chosen: WSM 6-class simple ice microphysics scheme (Hong and Lim 2006), unified Noah land-surface model (Chen and Dudhia 2001), BouLac boundary layer scheme (Bougeault

and Lacarrère 1989), Grell–Devenyi cumulus convection scheme (Grell and Devenyi 2002), RRTM longwave radiation (Mlawer et al. 1997), and Goddard shortwave radiation scheme (Chou and Suarez 1999). The initial and boundary conditions of the model are derived from ECMWF 6-hourly data (four times a day at 00:00, 06:00, 12:00, 18:00) at a horizontal resolution of  $2.5^\circ \times 2.5^\circ$ .

## 3 Spatiotemporal characteristics of Meiyu belt precipitation and rainstorm frequency in the YRB

Considering the seasonality of the Meiyu precipitation over East China, we first calculate the histogram of monthly average rainfall (Fig. 2a) and rainstorm frequency (Fig. 2b) over the YRB (106°–120°E, 28°–34°N) from 1979 to 2014. Results show that the highest precipitation and rainstorm frequency occur in June and July, and the seasonal characteristics of rainstorm frequency in July are especially significant. In addition, Fig. 2c shows the spatial distribution of climatological rainfall in July in East China (south of 40°N) from 1979 to 2014, and Fig. 2d shows the distribution of the rainstorm frequency. The precipitation shows a peak in July with high rainstorm occurrence in the YRB. During the largest floods in 1998, the YRB was located within a core zone with the highest rainstorm frequency within the zonally elongate Meiyu belt (Fig. 2e). Considering the distribution of extreme precipitation and rainstorm frequency, the YRB is chosen as the key research area (Zone A in Fig. 2c, 106°–120°E, 28°–34°N) for data analysis and model simulation.

## 4 Upstream “sensitivity area” of land-atmosphere process “strong signal” over the TP

Tracking the upstream “sensitivity area” over the TP for the Meiyu and rainstorms over the YRB is the key to studying the development of heavy rainfall in this region. Through analysis of the correlation between the average precipitation over the YRB in July during 1979–2014 and the SLHF over East Asia, we found that precipitation over the YRB is correlated with the SLHF over the TP. A zone of high correlation (significant at the 90% confidence level) is located at the SEMTP (zone B, 98°–105°E, 23°–32.5°N) (Fig. 3a). We therefore focus on the relationship between the upstream “strong signal” of SLHF over the SEMTP and the occurrence and development of the Meiyu rain belt over the YRB in July. In addition, the SEMTP is also the key observational region of the JICA-TP observation system.

Figure 3b, c show that there is a significant negative correlation band between domain-averaged SLHF over the

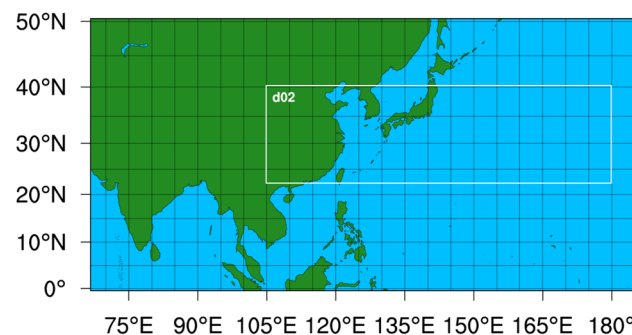


**Fig. 1** WRF model domain and nested model grid (d02)

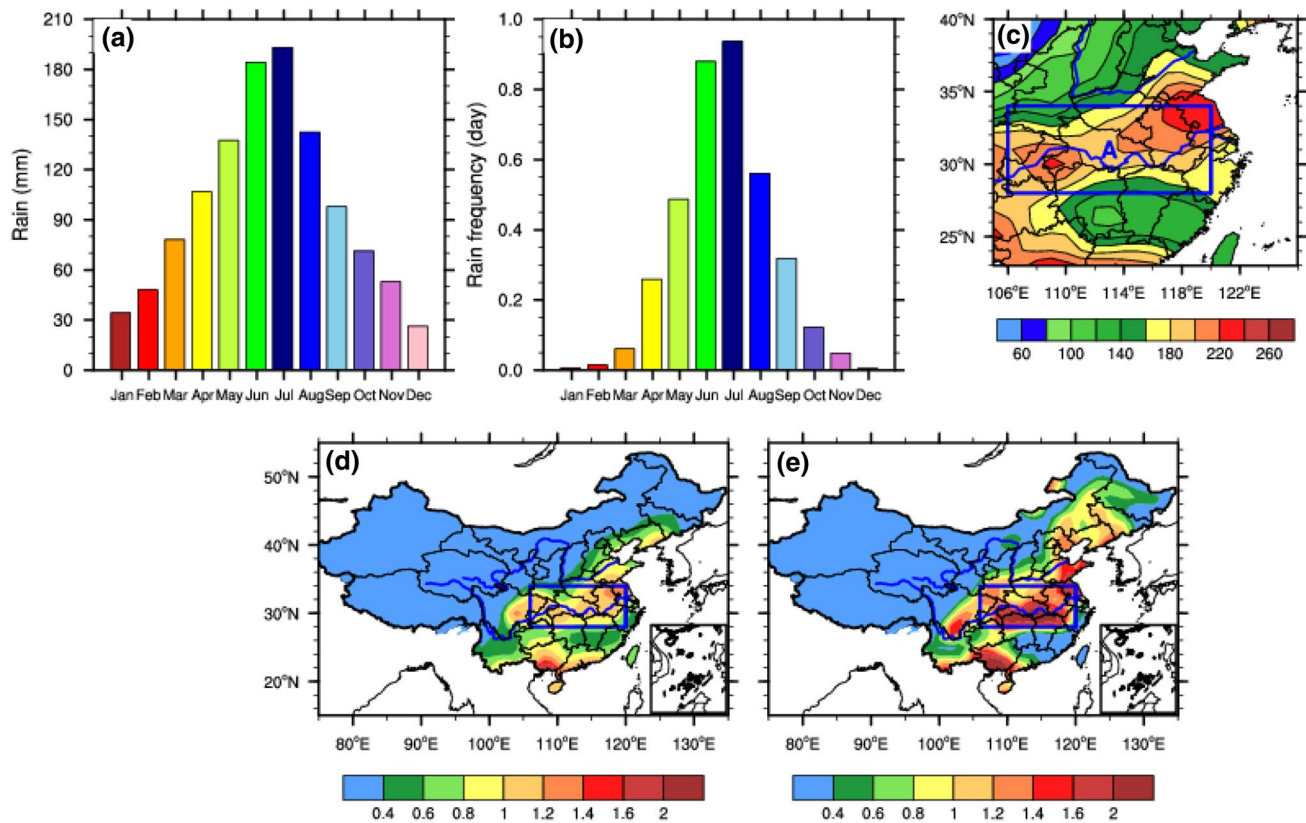
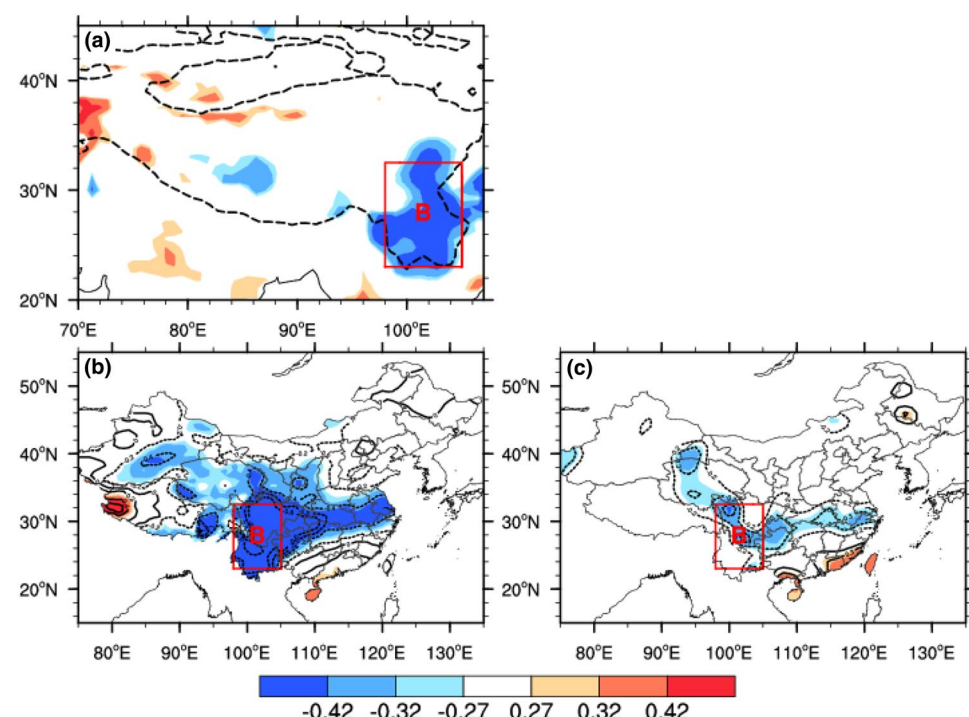


**Fig. 2** **a** Mean seasonal evolution of precipitation over the YRB (Zone A: 106°–120°E, 28°–34°N) for the period 1979–2014 (unit: mm); **b** as for **a**, but for rainstorm frequency (unit: day); **c** spatial distribution of 1979–2014 mean precipitation during July over East

China (unit: mm); **d** spatial distribution of 1979–2014 mean rainstorm frequency in July over China (unit: day); and **e** as for **d**, but for July 1998 (unit: day). Zone A in **c** is the key research area (106°–120°E, 28°–34°N)

**Fig. 3** **a** Spatial distribution of correlation coefficient between domain-averaged precipitation over the YRB and SLHF over the TP and surrounding areas in July during 1979–2014; the dashed black curve denotes the area of the TP above 1500 m; **b** spatial distribution of correlation coefficient between domain-averaged SLHF over the SEMTP and low cloud cover in China in July during 1979–2014; **c** spatial distribution of correlation coefficient between domain-averaged SLHF over the SEMTP and precipitation over China in July during 1979–2014. Shaded area in **a**–**c** denotes statistically significance at the 90% confidence level based on Student's *t* test. zone B (98°–105°E, 23°–32.5°N) is the SEMTP



SEMP and low cloud cover and precipitation over the YRB. This negative zone extends from the SEMTP to the YRB, indicating that the low cloud cover and precipitation over the YRB increase (decrease) when the SLHF weakens (strengthens) in the SEMTP. That is, the SLHF over the SEMTP is significantly correlated with the convective activity and precipitation of the Meiyu belt in the YRB.

To further confirm the connection between the upstream “strong signal” of SLHF over the SEMTP and extreme

weather events such as droughts and floods in the YRB, the correlation between SLHF over SEMTP and Meiyu rainfall over the YRB in July during 1979–2014 is calculated. The two time series are highly negatively correlated with correlation coefficients reaching  $-0.61$ , which is significant at the 99% confidence level using Student's *t* test (Fig. 4a). It is also found that the precipitation and rainstorm frequency in the YRB are out of phase with the inter-annual variation of SLHF over the SEMTP after normalization of both data

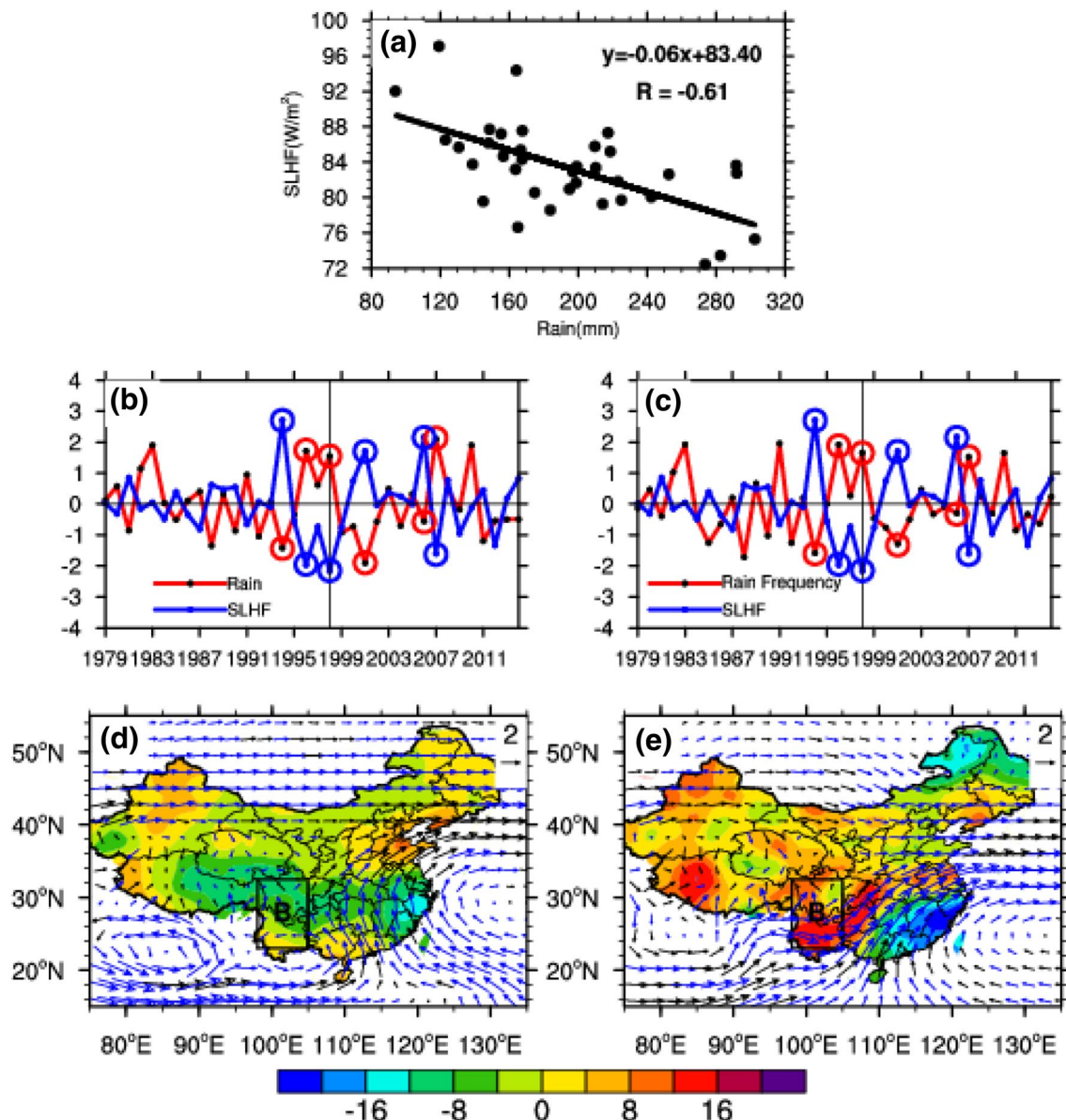


**Fig. 4** **a** Correlation model between precipitation over the YRB and SLHF over the SEMTP in July over the period 1979–2014; **b** standardized inter-annual variability of precipitation over the YRB and SLHF over the SEMTP; **c** standardized inter-annual variability of rainstorm frequency over the YRB and SLHF over the SEMTP (years with anomalously YRB precipitation are circled in red and years with anomalously SLHF over the SEMTP are circled in blue); **d** moisture

transport flux at 500 hPa (vectors, blue vectors indicate statistically significance at 90% confidence level, unit:  $\text{gs}^{-1} \text{hPa}^{-1} \text{cm}^{-1}$ ) and low level cloud cover anomaly (shading, unit: %) in July for the years 1994, 2001 and 2006 with anomalously high SLHF over the SEMTP; **e** the same as **d**, but for the years 1998, 1996, and 2007 with anomalously low SLHF over the SEMTP

sets according to Eq. (1). For example, in 1998 when SLHF was low ( $72 \text{ Wm}^{-2}$ ), the rainstorm frequency over the YRB during the Meiyu period was anomalously high with heavy rainfall (Fig. 4b, c) and precipitation over 273 mm. In contrast, the SLHF was anomalously high in 1994, 2001 and 2006, about 1.3 times that of 1998, at 97, 92 and 94  $\text{Wm}^{-2}$ , respectively.

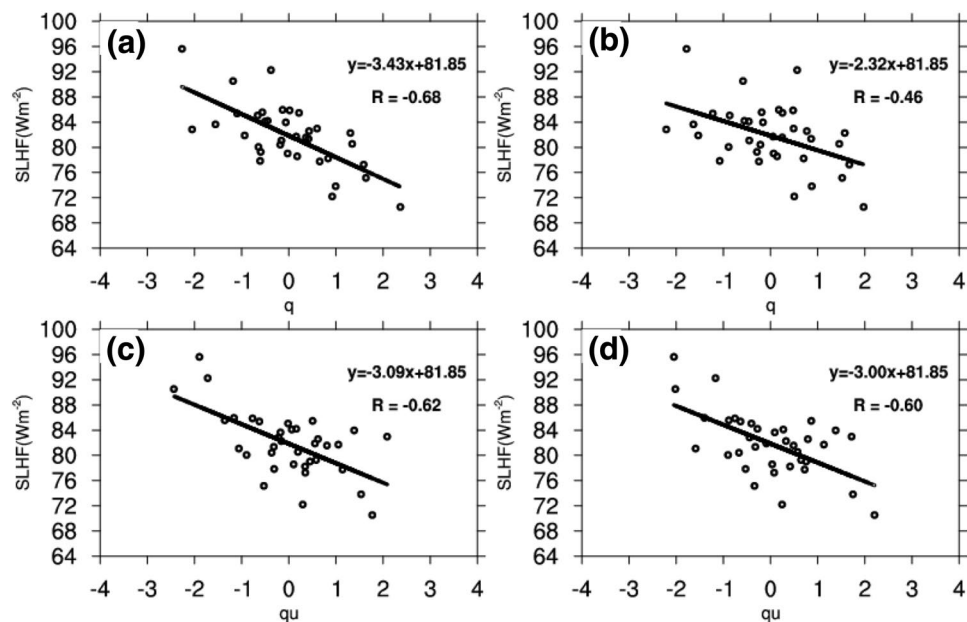
According to the negative correlation between SLHF over the SEMTP and the anomalous precipitation over the YRB, the following typical years characterized by anomalous SLHF and precipitation were selected: 1998, 1996 and 2007 with anomalously low SLHF over the SEMTP and high precipitation and storm frequency over the YRB; and 1994, 2001 and 2006 with anomalously high SLHF over the SEMTP and low precipitation and storm frequency over the YRB according to Eq. (1) (hollow circles in Fig. 4b, c). Figure 4d, e are composites showing the 500 hPa moisture transport flux and low level cloud cover anomaly in July for these typical years. In years with anomalously high SLHF (Fig. 4d), moisture from the low latitude oceans continues to move northward from east of the SEMTP and turns eastward at middle latitudes, leading to the anomalous low level zonal cloud band in Northern China. In contrast, in years with anomalously low SLHF (Fig. 4e), the moisture tends to turn eastward from east of the SEMTP resulting in the anomalous low level zonal cloud cover over the YRB and associated convective activity.

Figure 5a–d indicate that the SLHF over the SEMTP is negatively correlated with humidity at upper levels (600 hPa, 700 hPa) (Fig. 5a, b) and zonal moisture

transport ( $qu$ ) (Fig. 5c, d). Thus, when SLHF over the SEMTP is anomalously low (high), humidity at upper levels is high (low) and zonal moisture transport is strong (weak).

The above results reveal the monthly relationship between the low (high) SLHF over the SEMTP and high (low) humidity and zonal moisture transport at upper levels, as well as the high (low) precipitation and rainstorm frequency in the YRB. However, it is important to further explore the relationship between the low (high) SLHF over the SEMTP and the eastward (northward) movement of precipitation systems out of the SEMTP on synoptic scales, and thus identify the “strong signal” characteristic of the SEMTP for the evolution of downstream weather systems in the YRB. The daily SLHF over the SEMTP in July 1994, 2001 and 2006 (anomalously high SLHF) and 1998, 1996 and 2007 (anomalously low SLHF) was selected according to Eq. (1). Figure 6a, d show the correlation field between SLHF over the SEMTP and precipitation and moisture transport flux (3-day lag) according to Eq. (3) for low and high SLHF, respectively. The locations of the precipitation systems and patterns of the moisture transport that moves out from the TP are significantly different in these two cases after three days. Northward (eastward) movement of the moisture transport flux corresponds to high (low) SLHF. In addition, different locations of the precipitation systems and patterns of the moisture flux are more significant when using the data with 4- (Fig. 6b, e) and 5-day (Fig. 6c, f) lag. That is, the SLHF over the SEMTP relates to the moisture transport flux and precipitation over the YRB after about 3–5 days.

**Fig. 5** **a** Correlation model between SLHF over the SEMTP and 600 hPa specific humidity in July during 1979–2014; **b** the same as **a** but for 700 hPa; **c** correlation between SLHF over SEMTP and 600 hPa zonal moisture transport ( $qu$ ) during July 1979–2014; **d** the same as **c** but for 700 hPa



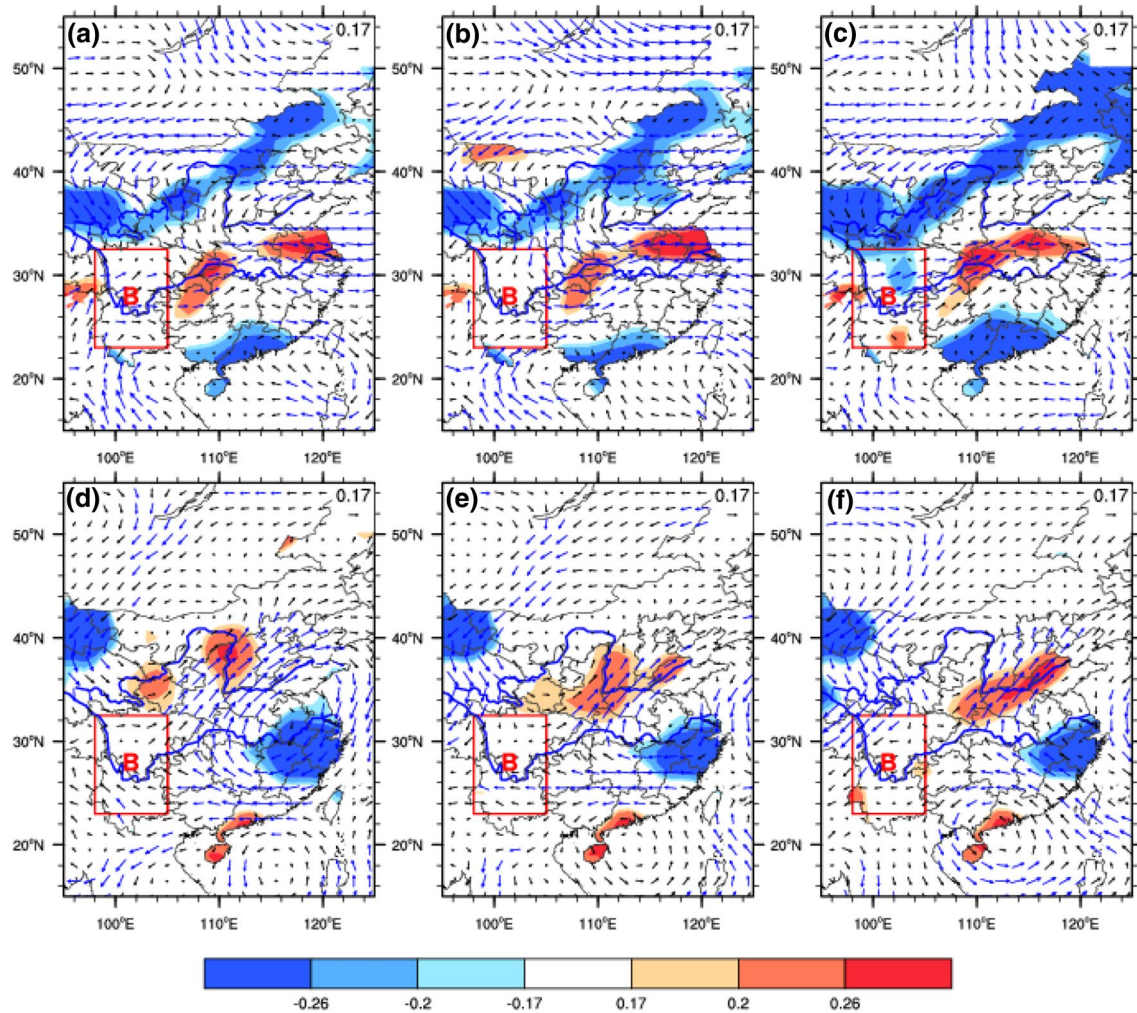


**Fig. 6** **a** Correlation field between SLHF over the SEMTP and 3-day lag 500 hPa moisture flux (vectors, blue vectors indicate statistically significance at 90% confidence level) and precipitation (shading, shaded areas indicate statistically significance at 90% confidence

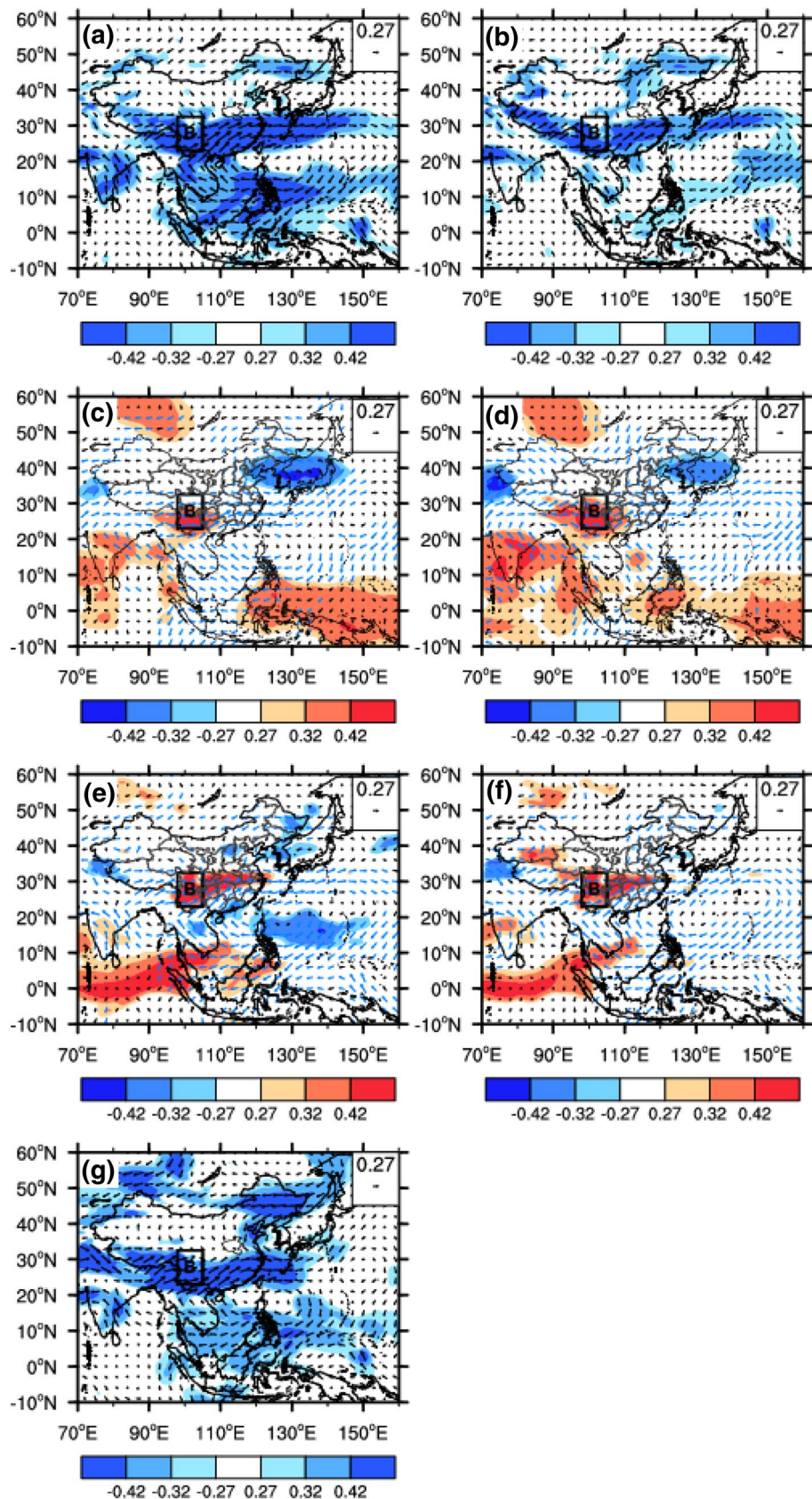
level) in July for low SLHF years 1998, 1996 and 2007; **b** the same as **a** but for 4-day lag; **c** the same as **b** but for 5-day lag; **d** the same as **a** but in July for high SLHF years 1994, 2001 and 2006; **e** the same as **d** but for 4-day lag; **f** the same as **e** but for 5-day lag

## 5 Relationship between SLHF in the “sensitivity area” over the TP and moist flow transport of the precipitation over the YRB

The moisture transport of the Meiyu belt over the YRB is characterized by interactions between the thermodynamic structure over the TP, the EAM system, and the sea-land-atmosphere processes at low latitudes. Therefore, it is important to further explore how the SEMTP over the TP relates the moisture transport from the low-latitude oceans, and contributes to the Meiyu anomaly and continuous rainstorm precipitation over the YRB. The correlation between the rainfall (rainstorm frequency) in the YRB in July and the moisture transport flux in East Asia according to Eq. (3) is shown in Fig. 7a, b. Figure 7a, b show that during heavy

precipitation rainstorms over the YRB in July, two branches (westerly and southerly) of correlation vectors of the moisture transport converge over the SEMTP. The westerly moisture flow originates from the Arabian Sea, whereas the southerly moisture originates from the South China Sea and the Bay of Bengal. In addition, as shown in Fig. 7c, d, the correlation field between the precipitation or rainstorm frequency in the YRB and the 500 hPa temperature field reveals a region of high correlation (warm southerly airflow) extending from the low latitude ocean northward to the SEMTP. Note that the correlations between rainstorm frequency and the 500 hPa temperature field (Fig. 7d) are more pronounced than that for rainfall in the YRB (Fig. 7c); i.e., the region with 90% confidence level is expanded significantly. This suggests that the environmental conditions associated with the extremely heavy rainfall are closely related to the warm

**Fig. 7** **a** Spatial distribution of correlation coefficient between precipitation over the YRB and integrated moisture transport flux over East Asia (vectors); **b** the same as **a**, but for torrential rainstorm frequency (daily precipitation  $\geq 100$  mm); **c** spatial distribution of correlation coefficient between precipitation over the YRB and 500 hPa temperature (shading) and 500 hPa moisture transport (vectors) over East Asia; **d** the same as **c**, but for torrential rainstorm frequency (daily precipitation  $\geq 100$  mm); **e** spatial distribution of correlation coefficient between precipitation over the YRB and integrated moisture transport (shading) and integrated moisture transport (vectors) over East Asia; **f** the same as **e**, but for torrential rainstorm frequency (daily precipitation  $\geq 100$  mm); **g** spatial distribution of correlation coefficient between the SLHF over the SEMTP (multiplied by -1) and integrated moisture transport (vectors). Shaded area in **a**–**g** indicate statistically significance at the 90% confidence level, blue vectors in **c**–**f** indicate statistically significance at 90% confidence level



and humid air flow extending from the low latitude ocean to the SEMTP. The cold air farther west over the western Himalayas in the mid-latitudes is also more pronounced than that over the northern Meiyu region. In addition, Fig. 7e, f suggest that the integrated moisture transport in the SEMTP and its belt-shaped pathway play an important role in influencing the downstream precipitation, as such a structure is more favorable to frequent heavy rainfall events in the YRB.

The above study reveals a clear relationship between the Meiyu precipitation over the YRB and the upstream moisture transport from the SEMTP and low latitude ocean. According to Xu et al. (2008a), both the integrated moisture transport ( $qu$ ,  $qv$ ) and the convective cloud activity (represented by black body temperature,  $T_{bb}$ ) over East Asia are highly correlated with the total apparent heat source (Q1) over the TP. This suggests that the thermal condition of the TP probably exerts an important effect on the precipitation over the YRB through modulating the upstream moisture transport.

The vector field of correlations between the SLHF (multiplied by  $-1$ ) over the SEMTP and the integrated moisture transport flux (Fig. 7g) can also describe a similar correlation structure of moisture transport associated with Meiyu rainfall and rainstorm frequency. The vectors related to the westerly and southerly moisture flows both converge on the SEMTP. The westerly moisture flow originates from the Arabian Sea while the southerly flow originates from the South China Sea and Bay of Bengal. The low-latitude ocean southerly moisture flow merges with the westerly moisture flow over the TP at the SEMTP, forming the upstream moisture transport of the Meiyu belt over the YRB. The above results confirm that the SEMTP is the key upstream “sensitivity area” for the occurrence and development of the Meiyu rain belt and associated rainstorms over the YRB. This “sensitivity area” is located in the key area of upstream moisture transport over the YRB. The SLHF over the “sensitivity area” and the corresponding structure of warm moisture transport play an important role in the water cycle of the anomalous precipitation over the YRB.

## 6 Correlated characteristics between the “strong signal” in the “sensitivity area” (the SEMTP) and the moisture circulation pattern around the subtropical high

The ridge of moisture transport of the Meiyu belt is defined as the latitude where the zonal mean moisture transport turns from westward to eastward between  $110^{\circ}$  and  $135^{\circ}\text{E}$  in July. As shown in Table 1 and Fig. 4e, the anomalously low SLHF in the SEMTP in 1998, 1996 and 2007 corresponds to anomalously higher precipitation in the YRB. The moisture transport over the YRB is strong and the average location of the ridge in these years is near  $22.5^{\circ}\text{N}$  (Fig. 4e). The anomalously high SLHF in the “sensitivity area” in 1994, 2001 and 2006 corresponds to anomalously lower precipitation in the YRB. The moisture transport and rain belt are located anomalously northward and the average location of the ridge in the high SLHF years is much farther north near  $29.5^{\circ}\text{N}$  (Fig. 4d). Further research indicated that SLHF in the “sensitivity area” is significantly correlated with the location of the ridge of moisture transport in the Meiyu period (99% confidence interval) (Fig. 8a, b). In addition, the “strong signal” of SLHF in the “sensitivity area” affects not only the precipitation but also the rainstorm and torrential rainstorm frequency in the YRB (Table 1). These results indicate that the “strong signal” of SLHF in the “sensitivity area” is highly related to both the belt-shaped moisture transport upstream of East China, and the location of the ridge of subtropical high moisture transport. Low SLHF in the “sensitivity area” accompanies more southward location of the ridge in East China. The warm, humid airflow passing from east of the “sensitivity area” favors more Meiyu rainfall and torrential rainstorms. In contrast, high SLHF in the “sensitivity area” accompanies with more northward location of the ridge in East China that favors frequent rainstorms in Northern China. On inter-annual time scales, low (high) SLHF in the “sensitivity area” corresponds to high (low) humidity and strong (weak) zonal moisture transport at upper levels and a

**Table 1** Precipitation, rainfall frequency and position of 500 hPa ridge of moisture transport over the YRB in anomalous years of SLHF over the SEMTP

SLHF	Year	SLHF over the SEMTP ( $\text{W/m}^2$ )	Precipitation in YRB (mm) [ $> 50 \text{ mm}$ , $> 100 \text{ mm}$ ] rainfall frequency in the YRB (day/month)]	500 hPa ridge of moisture transport circulation
Anomalously low	1998	72	273 (1.59, 0.31)	$19.5^{\circ}\text{N}$
	1996	73	282 (1.68, 0.53)	$24^{\circ}\text{N}$
	2007	75	302 (1.54, 0.36)	$24^{\circ}\text{N}$
Anomalously high	1994	97	119 (0.43, 0.08)	$32.25^{\circ}\text{N}$
	2001	92	93 (0.54, 0.04)	$29.25^{\circ}\text{N}$
	2006	94	164 (0.89, 0.1)	$27^{\circ}\text{N}$

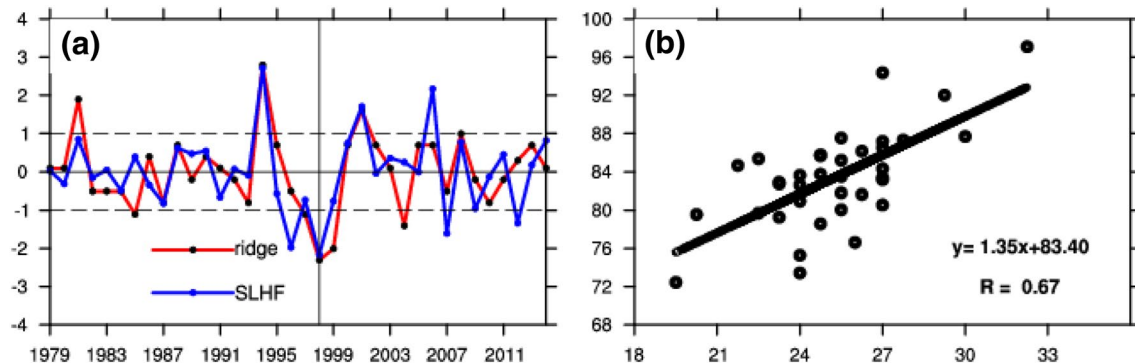


**Fig. 8** **a** Standardized inter-annual variability of ridge of 500 hPa moisture transport and SLHF over the SEMTP in July 1979–2014; **b** correlation model of ridge of 500 hPa moisture transport and SLHF over the SEMTP in July during 1979–2014

southward (northward) shift of the EASM moisture transport pattern. The two different EASM moisture transport patterns with anomalously eastward or northward turning of the moisture carried by the EASM when it flows from east of the “sensitivity area” transfer moisture to give a confluence of moisture flow originating from the mid-low latitude oceans. The SLHF reflects the “strong signal” feature of moisture transport structure in the “sensitivity area” and the variation of the position of the ridge of the subtropical high in the Meiyu period.

Previous research had shown that a strong heat source  $\langle Q_1 \rangle$  over the TP in summer is associated with anomalously high precipitation over the YRB in the same period (Luo and Chen 1995; Zhao and Chen 2001a). Chen et al. (2003) discovered that a stronger apparent heat source  $\langle Q_1 \rangle$  favors heavy precipitation over the YRB and a southward retreat of the subtropical high 7–9 days later by analyzing the daily apparent heat source  $\langle Q_1 \rangle$  over the TP and precipitation and the position of the subtropical high in East China after 7–9 days in the summer of 1998. Liu et al. (2002) analyzed the relationship between a heating index in the TP and the circulation in July. The results show that heating over the TP leads to a southward retreat of the subtropical high and airflow from the south and north converging over the YRB. Wu et al. (2016) studied the characteristics and interactions of surface sensible and latent heating over the TP using numerical simulations. Their results show that both the sensible and latent heating impact the thermal structure and flow field in the upper troposphere and can enhance the Asian monsoon circulation and the Northern Hemispheric circulation by generating Rossby waves that propagate in the westerlies.

Here we first calculate the correlation between the vector moisture transport flux field as given by the ECMWF 10 m moisture transport flux in July during 1979–2014 and the apparent heat source  $\langle Q_1 \rangle$  [according to Eq. (5)] in the TP ( $80^{\circ}$ – $105^{\circ}$ E,  $27.5^{\circ}$ – $37.5^{\circ}$ N) (Fig. 9a). The results show that when the apparent heat source  $\langle Q_1 \rangle$  over the TP is stronger,

cyclonic circulation in the TP and adjacent regions at the surface is enhanced. A stronger apparent heat source  $\langle Q_1 \rangle$  in the TP is related to abnormal southwesterly winds and a stronger EASM at the surface over the YRB. It is also related to heavy precipitation and rainstorms in the YRB in association with a subtropical high system circulation pattern lying farther south. These results are consistent with those of prior studies (Zhao and Chen 2001b).

Second, as shown above, the SLHF over the SEMTP has a “strong signal” characteristic for precipitation over the YRB and the location of the ridge of subtropical high pressure. Standardized inter-annual variations (Fig. 9b) and the correlation model (Fig. 9c) are calculated to further explore the relationship between the SLHF over the SEMTP and the apparent heat source  $\langle Q_1 \rangle$  field over the entire atmospheric column [according to Eq. (5)] in the TP ( $80^{\circ}$ – $105^{\circ}$ E,  $27.5^{\circ}$ – $37.5^{\circ}$ N). The results show that the two series are highly negatively correlated with correlation coefficient of  $-0.66$  at the 99% confidence level. The correlation field over the TP between SLHF over the SEMTP and the apparent heat source  $\langle Q_1 \rangle$  (Fig. 9d) shows an area of significant negative correlation (90% confidence interval) over the southeast, south slope and main body of the TP. Previous studies have shown that the latent heat release of cumulus convection is high at 400–500 hPa (He et al. 2011). In Fig. 9e there is a band of significant negative correlation between SLHF over the SEMTP and the 400 hPa apparent heat source  $Q_1$ . This negative zone extends from west to east of the TP and the negative correlation feature is more significant over the east of the TP than over its main body. He et al. (2011) analyzed the horizontal distribution of latent heating at 6 km altitude (about 400–500 hPa) during spring–summer 1998–2007. Their results show that the latent heat release over the southeastern TP is significantly stronger than that over the main body of the TP. This is consistent with the conclusion that the heating center of the TP is not located over its main body but over the southeast TP based on latent heating in

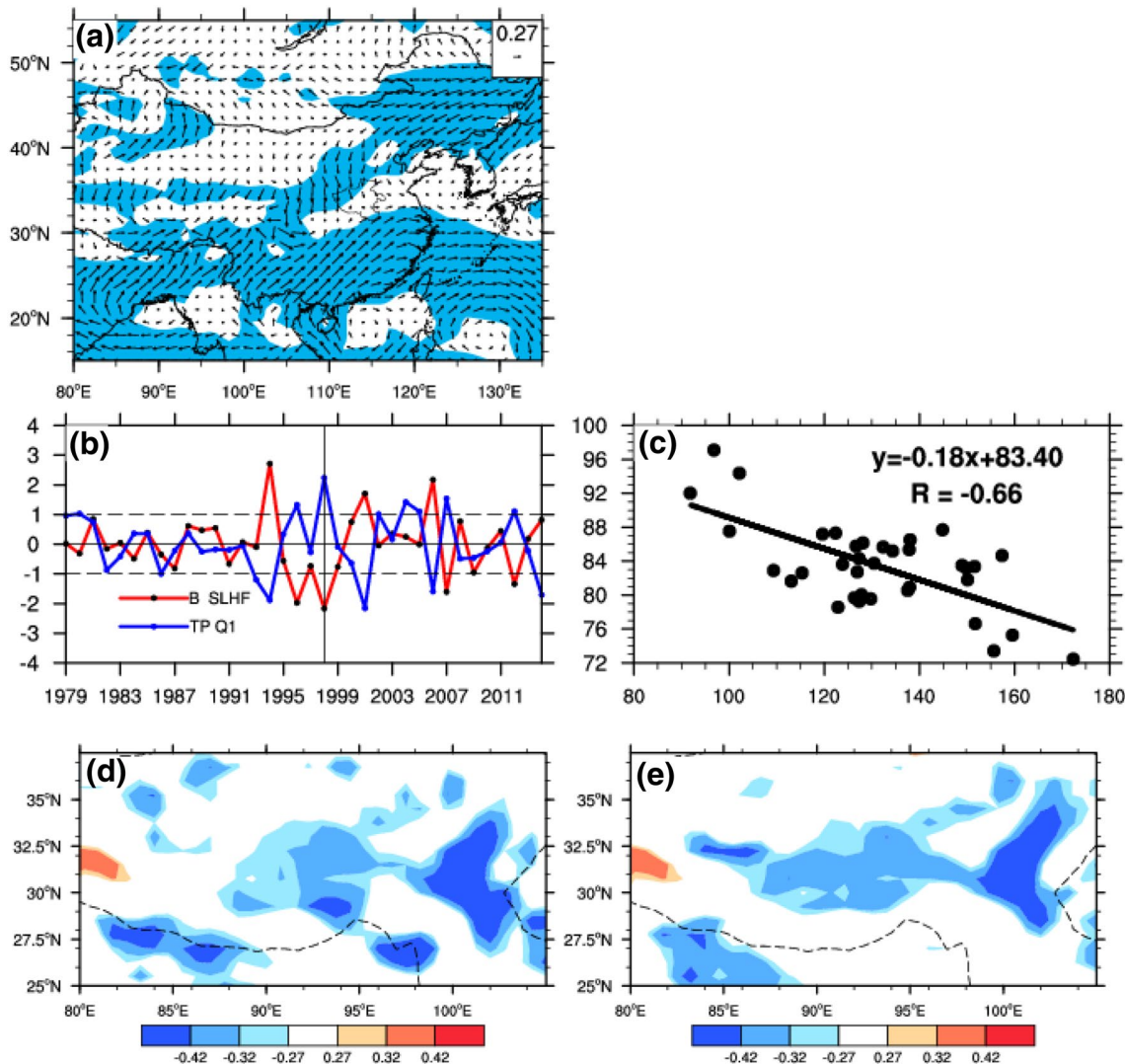


**Fig. 9** **a** Correlation vector distribution between apparent heat source  $\langle Q1 \rangle$  in the TP ( $80^{\circ}$ – $105^{\circ}$ E,  $27.5^{\circ}$ – $37.5^{\circ}$ N) and 10 m moisture transport flux in East Asia in July during 1979–2014 (vectors); **b** standarized inter-annual variation of the SLHF over the SEMTP and apparent heat source  $\langle Q1 \rangle$  over the TP; **c** the same as **b**, but for the correlation model; **d** correlation field over the TP between SLHF over

the SEMTP and the apparent heat source  $\langle Q1 \rangle$  field (shading); **e** the same as **d**, but for apparent heat source  $\langle Q1 \rangle$  at 400 hPa. Shaded area in (a, d and e) indicate statistically significance at the 90% confidence level, the dashed black curve in **d**–**e** denotes the area of the TP above 1500 m

summer (Chen et al. 1965). Condensation latent heating is the principal contributor to the apparent heat source  $\langle Q1 \rangle$  in summer (He et al. 2011). Therefore, when strong cumulus convection appears over the main body of the TP, the condensation latent heating increases within the cumulus clouds accompany with a stronger apparent heat source  $\langle Q1 \rangle$  over the entire atmospheric column. When the cloud system appears over the SEMTP, the thick clouds reduce the proportion of solar radiation reaching the ground. The daily variation of surface net radiation fluxes depends mainly on the variation of the downward short-wave radiation flux at the surface. Surface net radiation fluxes over the SEMTP decrease as the condensation latent heating increases in the

cumulus cloud over the main body of the TP (increasing the apparent heat source  $\langle Q1 \rangle$ ). The main energy source of SLHF is surface net radiation fluxes. An increasing in the apparent heat source  $\langle Q1 \rangle$  over the main body of the TP leads to decreasing SLHF over the SEMTP and a southward shift of the summer subtropical high system circulation pattern. The correlation field between daily  $\langle Q1 \rangle$  over the main body of the TP in July (1994, 2001, 2006, 1998, 1996 and 2007) and precipitation and 500 hPa moisture transport flux (1-, 2-, 3-day lag) indicates that the locations of the precipitation systems and the moisture transport that moves out from the TP to the SEMTP after one day. The precipitation systems and zonal moisture transport over YRB are more

significant after 2–3 days. In addition, very similar patterns are seen when using the data with the 4-, 5-day lag (figure not shown). That is, the  $\langle Q \rangle$  relates to the moisture transport flux and precipitation over the YRB about 2–5 days later. The above research confirms the conclusion that strong or weak SLHF over SEMTP is a “strong signal” feature for moisture transport in the YRB and for the position of the subtropical high system circulation. The possible driver is the increase in the apparent heat source  $\langle Q \rangle$  over the main body of the TP as mentioned earlier.

## 7 Numerical experiment and analysis of simulation results

### 7.1 FLEXPART particle dispersion model analysis

To further confirm the SEMTP as the upstream critical area for the moisture transport of the Meiyu belt in the YRB, FLEXPART was used to calculate the forward trajectory of moisture particles over the SEMTP. ECMWF reanalysis data were used as the driving field. The particle swarm was initially placed over the SEMTP in the “sensitivity area”

(98°–105°E, 23°–32.5°N) and between 100 m and 6000 m altitude. The simulation period is from 00:00 on July 17, 1998 to 00:00 on July 23, 1998. The moisture particle swarm initially located in this region (the SEMTP) (Fig. 10a) left the plateau at 03:00 on July 18 and moved to the east of the YRB in Southwest China (Fig. 10b). At 06:00 on July 20, the particle swarm covered the YRB occupying a zonally elongated area (Fig. 10c). These results show that the moisture flow in the SEMTP in July 1998 showed a significantly zonally stretched distribution with its source located in the SEMTP.

### 7.2 Sensitivity experiment of SLHF “strong signal” over the “sensitivity area”

ECMWF reanalysis data from March 5, 2008 to July 6, 2009 and for July 2014–2016 were compared with insitu data from the boundary layer observation station at Dali. Figure 11a shows that the SLHF of the two data sets has significant positive correlation (correlation coefficient of 0.81 with 99% confidence level). Using the 3-hourly average data for July in 2014–2016, we found that the high correlation area is located in the SEMTP with 99% confidence level. The SLHF

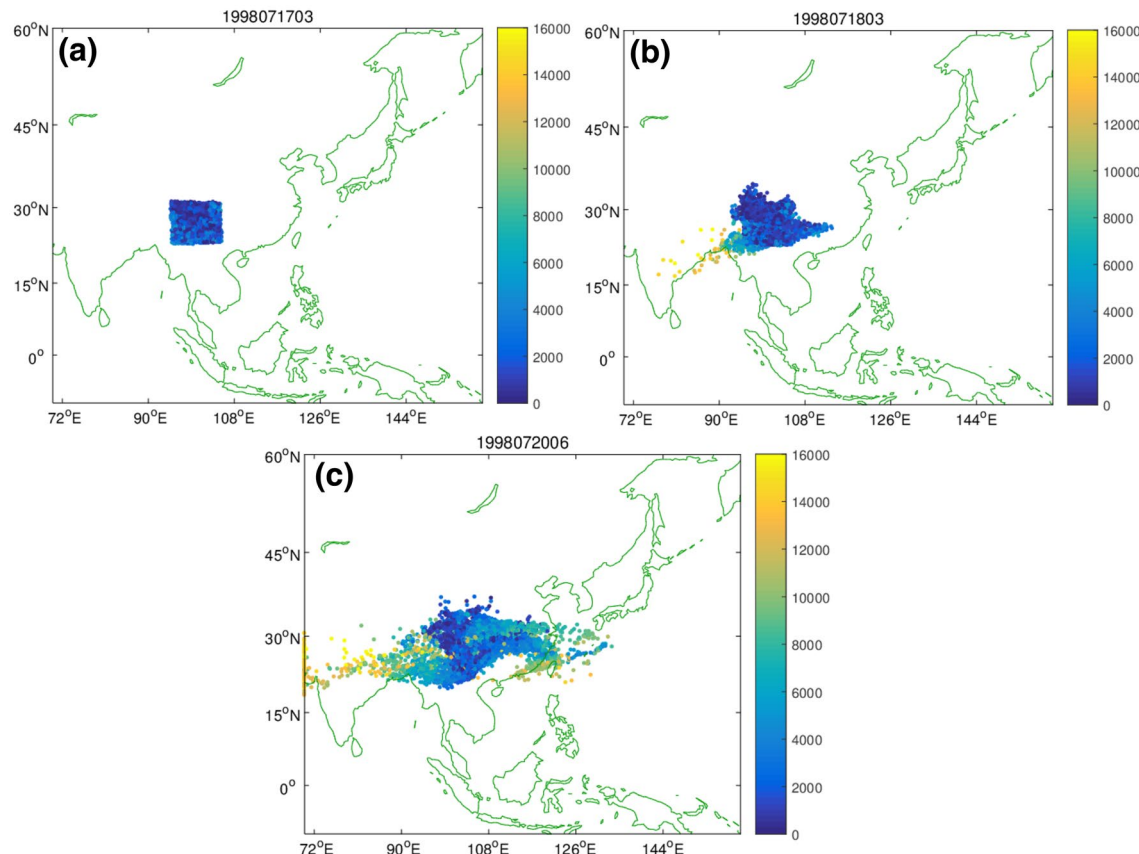


**Fig. 10** FLEXPART particle dispersion model analysis: moisture particle distribution at **a** 03:00 on July 17, **b** 03:00 on July 18, and **c** 06:00 on July 20

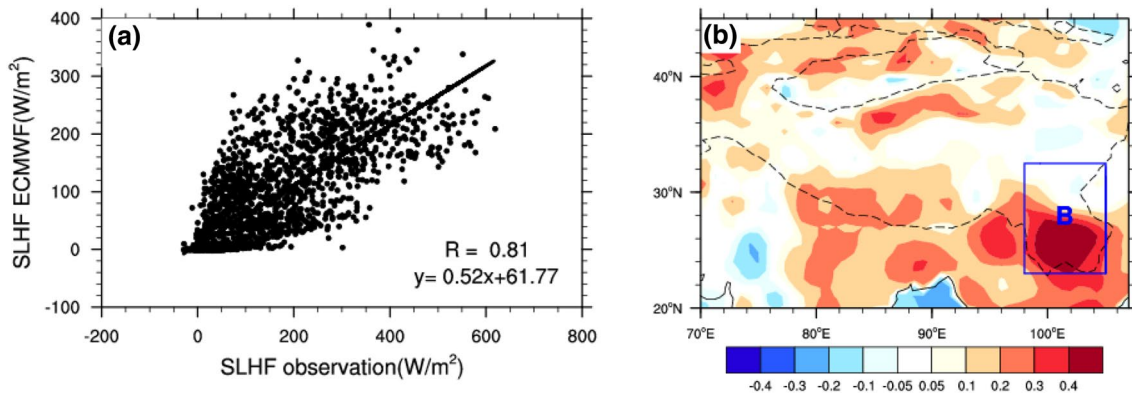


**Fig. 11** **a** Correlation model of the 3-hourly average SLHF over SEMTP and observational data from Dali station for March 5, 2008 to July 6, 2009 (unit:  $\text{Wm}^{-2}$ ); **b** correlation map of SLHF for July 2014–2016 between the data at the Dali station (3-hourly average)

from the two sets of data in the “sensitivity area” are consistent as point-to-surface representation; that is, the two sets of data are both good representations of the regional SLHF estimate over the SEMTP as shown in Fig. 11b. Therefore it is appropriate to use the ECMWF data for the analysis and numerical model simulation in this region.

The results so far describe the climatic correspondence between low (high) SLHF over the SEMTP and high (low) typical precipitation over the YRB. The SLHF is anomalously low in 1998 and anomalously high in 1994 (1.3 times that in 1998). In addition, in terms of synoptic scale features, the daily low (high) SLHF over the “sensitivity area” is negatively correlated with humidity at 600 hPa and 700 hPa. When the SLHF over the “sensitivity area” is low (high), the humidity is high (low) at the upper levels in July 1998 (not shown). The SLHF over the SEMTP relates to the moisture transport flux and precipitation over the YRB after about 3–5 days. This indicates that the moisture transport in the zonal belt-shaped domain is pronounced when the SLHF is low and favors more precipitation and frequent rainstorms in the YRB in the Meiyu period. The diagnostic analysis reveals that the variation of SLHF over SEMTP is a “strong signal” for the downstream weather systems and anomalous precipitation. We therefore test this hypothesis further by designing two sets of numerical simulations with a focus on the SEMTP: (1) control run (CTL), (2) experiment B: increasing the SLHF over SEMTP to 150% of the CTL (Table 2). The simulation period is from 00:00 on June 20 to 18:00 on July 31, 1998, the simulated results are used from 00:00 on July 1 to 18:00 on July 31. These cases are approached by increasing the SLHF of the SEMTP at each simulation time step in the land surface model to 150% of the CTL, while the land surface energy balance is kept unchanged (meaning the SLHF is still computed by the land model at each time step and allowed to impact land surface

and the ECMWF data during the same period (the shaded region with 99% confidence level, the dashed black curve denotes the area of the TP above 1500 m)

**Table 2** Design of numerical experiments

Case	Experiment design
CTL	Control experiment
B	Increasing the SLHF over SEMTP to 150% of CTL

moisture). Apart from the modified SLHF, other settings in experiment B are the same as in CTL.

### 7.2.1 Analysis of CTL simulation results

Figure 12b shows the CTL simulation results over July 1998. Simulated precipitation over the YRB and its downstream regions including the Korean Peninsula and Japan agrees well with CRU data (Fig. 12a). The spatial correlation coefficient between the observations and CTL is 0.52 in the YRB and 0.25 in the SEMTP. The root-mean-square errors are  $4.38 \text{ mm day}^{-1}$  and  $4.64 \text{ mm day}^{-1}$ , respectively. The results show that the WRF model reproduces the rainfall pattern reasonably well over the “sensitivity area”, the YRB and Southwest China during the Meiyu period of July 1998, suggesting that the model is suitable for the proposed experiment.

### 7.2.2 Sensitivity analysis of SLHF over the “sensitivity area” of the TP

Figure 13a shows the histogram of downstream percentage anomalies in accumulated precipitation in the sensitivity experiment B relative to CTL. Figure 13a shows that the accumulated precipitation over the YRB is reduced by 26% in experiment B. There are positive anomalies with respect to CTL in South China and the upper reaches

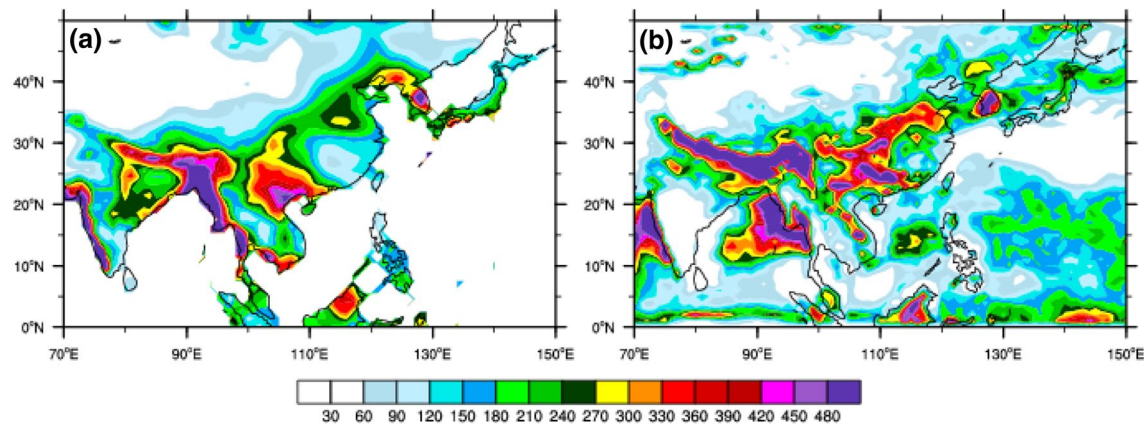


**Fig. 12** Accumulated rainfall (unit: mm) in July 1998 from **a** CRU observations; **b** the CTL simulation

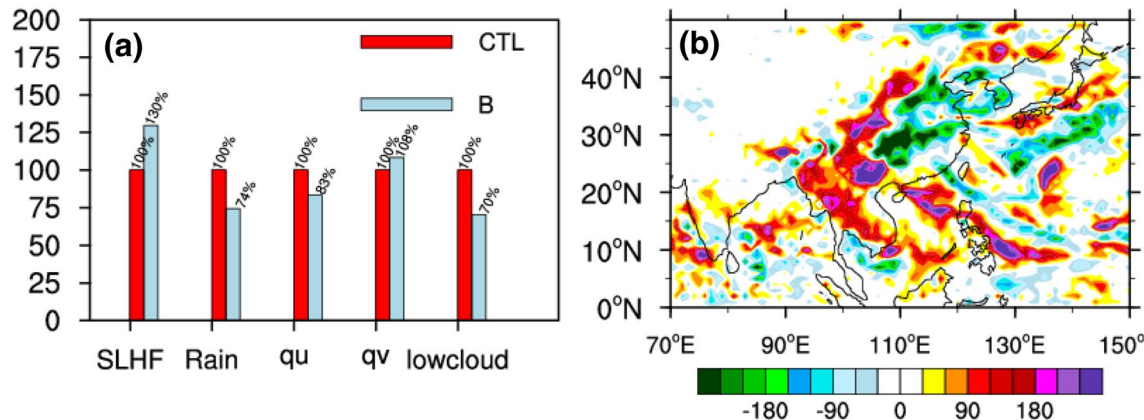


**Fig. 13** **a** Histogram of accumulated precipitation, integrated moisture transport (zonal and meridional components), and low level cloud cover anomaly percentages in the YRB in experiment B in

comparison to CTL (unit: %); **b** difference field of accumulative precipitation in July 1998 between experiment B and CTL (unit: mm)

of the YRB and Northern China (Fig. 13b). In addition, Fig. 13a also demonstrates that in the sensitivity experiment B, as the SLHF increases in the “sensitivity area”, the eastward component of moisture flow (*qu*) diverted into the YRB decreases. The low level cloud cover as well as the convective activity decrease correspondingly. Furthermore, the northward component of moisture flow (*qv*) increases. The results of the simulation also agree with the conclusion that the increase in SLHF over the SEMTP corresponds to a decrease in precipitation over the YRB. The above sensitivity experiment results are consistent with the conclusion that the northward moisture transport structure and precipitation belt are related to the anomalously high SLHF over the SEMTP (Fig. 4d).

### 7.2.3 Structure of moisture transport

Xu and Zhang (1999) showed that the Indian Ocean, the Bay of Bengal, and the South China Sea are the main monsoon moisture sources that affect the droughts and floods in China. The thermal forcing due to the special terrain of the TP and the associated moisture confluence make the TP a “transfer station” for the flow of monsoon moisture toward the YRB, and produces a moisture distribution characterized by specific patterns over the TP and the YRB in wet and dry years. The CTL simulation of the 500 hPa moisture transport flux (Fig. 14a) shows that there are three main moisture sources: the Arabian Sea, the Bay of Bengal, and the South China Sea. The moisture from the Arabian Sea,

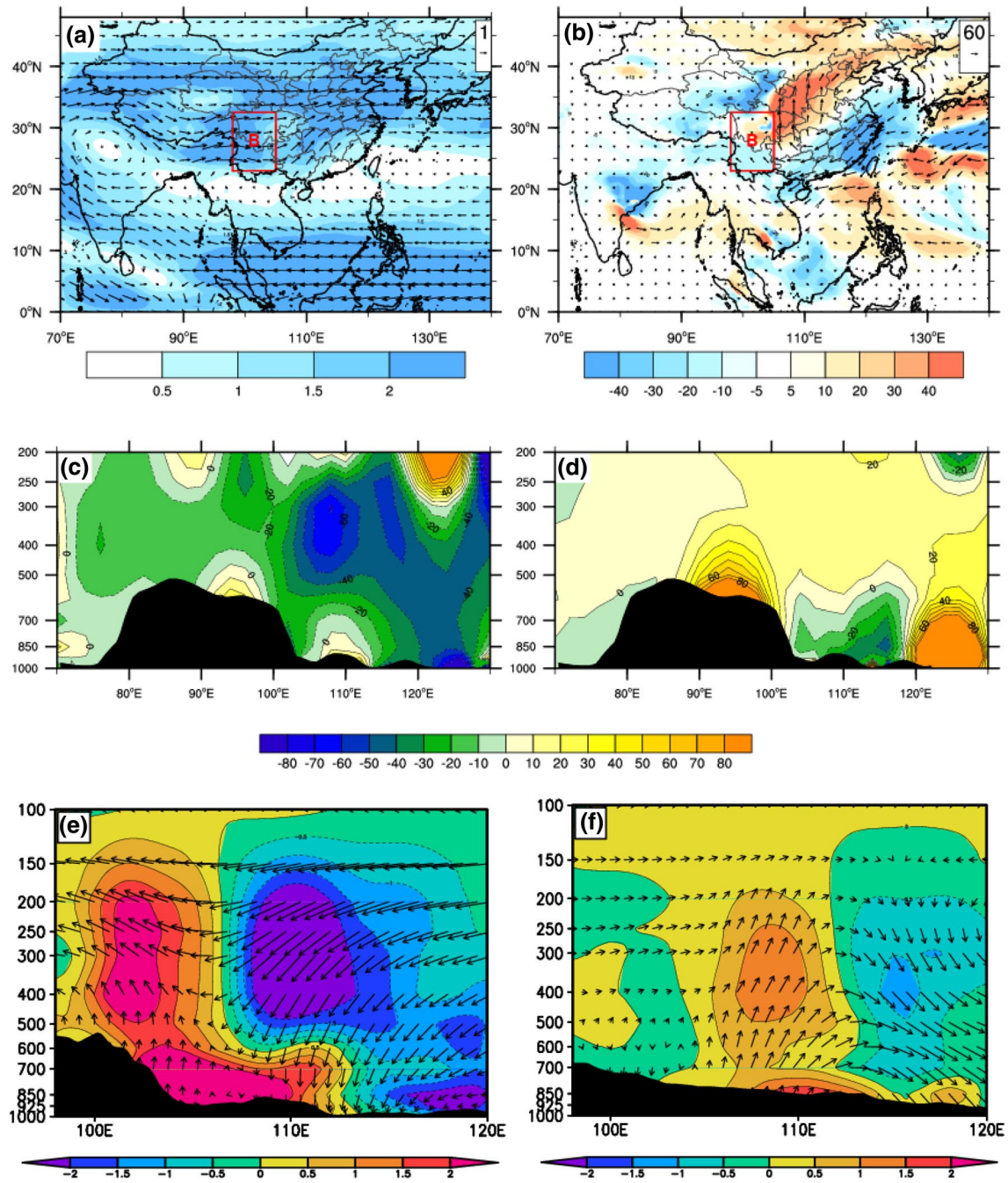


**Fig. 14** **a** Moisture transport (vectors) and moisture transport flux (shading, unit:  $\text{gs}^{-1} \text{ hPa}^{-1} \text{ cm}^{-1}$ ) at 500 hPa in CTL for July 1998; **b** differences field in integrated moisture flux between experiment B and CTL (unit:  $\text{gs}^{-1} \text{ hPa}^{-1} \text{ cm}^{-1}$ ); **c** zonal transect of the *qu* anomaly (averaged over 27.5°–32.5°N, unit: %) in experiment B relative to

CTL expressed as a percentage of the CTL value; **d** the same as **c**, but averaged over 35°–48°N; **e** the difference in zonal transect circulation (averaged over 27.5°–32.5°N) between experiment B and CTL; **f** the same as **e**, but averaged over 35°–48°N. Contours and shading in **e**, **f** indicate the average  $\omega$  anomaly (unit:  $10^{-6} \text{ Pa s}^{-1}$ )

the Bay of Bengal, and Indochina converge over the TP, flow through the SEMTP and turn eastward, while the moisture transport from the South China Sea turns sharply eastward at the SEMTP. The CTL simulation shows that the moisture from both the western and southern boundaries of the YRB makes important contributions to the Meiyu rainfall.

Experiment B further explored the SLHF over the “sensitivity area” related to the moisture transport to the YRB during the Meiyu period. The moisture transport flux anomalies in the B simulation relative to the CTL simulation show that moisture from the TP (over the western boundary of the YRB) and from the southern boundary of the YRB is

significantly reduced while the southwest moisture transport from the east of the SEMTP to Northern China is enhanced (Fig. 14b). The EASM moisture flows through the turning area from east of the SEMTP and turns northward. The zonal transect of the moisture transport anomaly for experiment B shows that the moisture transport carried by the westerlies between 500 hPa and 300 hPa over the region  $27.5^{\circ}$ – $32.5^{\circ}$ N decreases by > 40% (Fig. 14c) while the transport between the surface and 300 hPa over the region  $35^{\circ}$ – $48^{\circ}$ N increases by > 40% (Fig. 14d). The above results indicate that the moisture flow carried by the EASM during the Meiyu period is characterized by a northward deflection at the SEMTP when the SLHF over the SEMTP is enhanced.

#### 7.2.4 Structure of the vertical circulation

To further analyze the relationship between SLHF over the “sensitivity area” located in the SEMTP and the convective precipitation over the YRB, the meridional and zonal transects of the vertical circulation anomalies of experiment B are analyzed (Fig. 14e, f). When the SLHF over SEMTP is increased by 150% (experiment B), the results show that the average zonal circulation in the YRB weakened between  $27.5^{\circ}$  and  $32.5^{\circ}$ N (Fig. 14e), and significant anomalous downwelling was observed in the region east of  $105^{\circ}$ E, while over  $35^{\circ}$ – $48^{\circ}$ N north of the YRB (Northeast China), the average zonal circulation is enhanced and anomalous upwelling is observed around  $105^{\circ}$ – $110^{\circ}$ E (Fig. 14f). The above results show that these changes in the circulation anomaly in East China correspond to the increase of SLHF over SEMTP. That is, the change of SLHF over the SEMTP is significantly related to the convective activity in the YRB, which is also related to moisture transport during the Meiyu period.

#### 7.2.5 Characteristics of cloud structure

In summer, the dynamics and the thermal forcing of the TP not only play an important role in the formation of the monsoon circulation and precipitation, but also have an important impact on the development of weather systems in East China (Tao and Ding 1980; Tao et al. 1998; Yanai et al. 1992; Wu and Zhang 1998). Xu et al. (2001) and Wang et al. (2003) found that cloud systems that develop over the TP can be strengthened into deep convective cloud clusters as they move eastward and contribute to China’s summer monsoon precipitation. They also pointed out that the TP is an important source of convective cloud systems causing floods in the middle and lower reaches of the Yangtze River. Based on the analysis of satellite cloud images of torrential rain over the YRB in June–July 1998, the trajectory of the cloud system responsible for the floods in the YRB were found and can be traced to the central and eastern regions of the TP,

where “popcorn” convective clouds can often be observed (Xu et al. 2002b). In years of high SLHF over the “sensitivity area”, when the crest line of the subtropical high moves farther north, there is anomalously extensive low level cloud cover (> 4%) in the northern and northeastern regions, while cloud cover is anomalously low over the YRB. In years of low SLHF over the SEMTP there is a strong zonal moisture transport over the SEMTP and the YRB is characterized by strong moisture south–north convergence in the middle and low latitudes with a strong zonal transport. Furthermore, the anomalously extensive (> 12%) low level cloud cover stretches from the SEMTP to the YRB (Fig. 4d, e). This is consistent with the moisture convergence zone discussed above. This indicates that anomalously strong (weak) SLHF over the SEMTP is highly correlated with eastward (northward) deflection of moisture carried by the EASM as well as the distribution of low level cloud cover anomaly during the Meiyu period over the YRB. The results of the zonal transect of cloud cover anomaly (average over  $27.5^{\circ}$ – $32.5^{\circ}$ N) in experiment B show that when the SLHF over the “sensitivity area” increases, the cloud cover in the region east of  $110^{\circ}$ E decreases significantly, especially below 500 hPa, where the cloud cover reduces by more than 50% (figure omitted). The simulation results further confirm that the SLHF over the SEMTP plays an important role in the “strong signal” of the convective activity and cloud cover in the YRB.

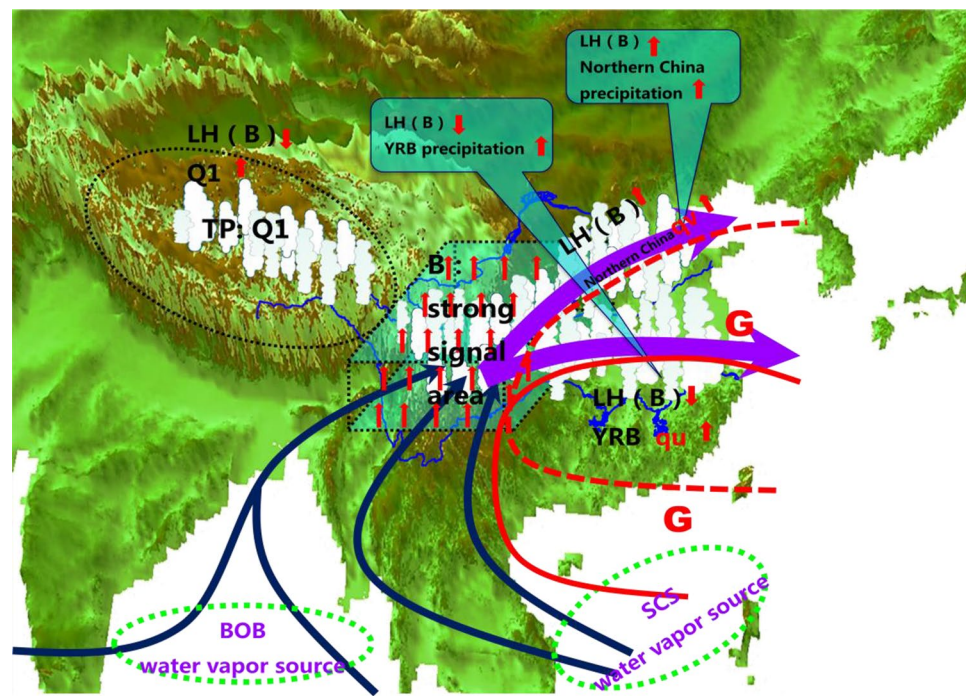
To verify the robustness of the conclusions obtained from the 1998 case study, similar numerical experiments were performed for 1996 and 2007, years with negative SLHF anomaly over the SEMTP and typical flooding in the YRB in July. The simulation results also agree with the conclusion that increasing SLHF over the SEMTP corresponds to decreasing precipitation over the YRB. The results of above sensitivity experiments are consistent with the conclusions of July 1998 (figure not shown). This case study provides further evidence that the SLHF over SEMTP plays an important role in the “strong signal” of upstream moisture transport and the precipitation belt.

## 8 Conclusions and discussion

The relationship between the upstream “strong signal” of the SLHF over the “sensitivity area” (the SEMTP) and the Meiyu precipitation and associated moisture transport over the YRB have been explored. In July 1998, severe floods occurred in a zonally elongated zone of the Meiyu belt in East China. There is a significant correlation between the disastrous floods in the YRB and the “strong signal” of the land–atmosphere processes in the SEMTP driven by specific circulation patterns at mid and low latitudes.

Precipitation over the Meiyu region of the YRB is closely related to the relatively warm and humid flow extending

**Fig. 15** Schematic showing the physical processes driving the anomalous precipitation over East China and the upstream SLHF “strong signal” in the “sensitivity area”



from the low latitude oceans to the “sensitivity area”. Rain-storm frequency has a stronger correlation than rainfall with the southerly warm airflow. The “strong signal” in the SEMTP reflects strong or weak moisture transport along the flank of the subtropical high system. It can also reveal collaborative effects between the special circulation pattern in the Meiyu belt and thermodynamic effects in the TP. The correlation between the integrated moisture transport flux in the “sensitivity area” and the belt-shaped zone of strong flux downstream is also important as such a structure is more favorable to frequent heavy rainfall events in the YRB.

During the years with high and low anomalous precipitation over the YRB, convective activities and moisture flow showed different upstream and downstream circulation patterns. Low (high) SLHF over the SEMTP is associated with high (low) humidity at upper levels and strong (weak) zonal moisture transport and corresponding high (low) precipitation and rainstorms in the YRB under the background of a southward (northward) shifted subtropical high system. The warm, humid airflow from the low latitude oceans is strong (weak) when it passes from east of the SEMTP; the moisture convergence is strong (weak) over the YRB and convection is significant (insignificant). Furthermore, the moisture flow responsible for the high precipitation over the Meiyu belt originates from the South China Sea, Indochina Peninsula, and Bay of Bengal and moves through the TP before turning toward the YRB. The key turning area is located in the “sensitivity area” (SEMTP) (Fig. 15).

Taking the typical flood year 1998 during the Meiyu period as an example, the WRF model simulation results

confirm that the SEMTP is the key upstream “sensitivity area” and SLHF is a “strong signal” for the formation and development of the Meiyu belt and associated heavy rainfall in the YRB. Sensitivity analyses based on the mesoscale model further reveal that a strong or weak SLHF over the “sensitivity area” reveals the change of the structure of moisture transport in East China. This “strong signal” could reflect the location of the subtropical high system in the Meiyu period and changes in the rainfall distribution pattern in East China.

This work has focused on the relationship between land-atmospheric process anomalies over the SEMTP and the precipitation over the YRB and associated circulation anomalies in July. However, other factors, such as SST anomalies in winter and spring (e.g., Li et al. 2017b; Fang et al. 2018), snow anomalies in Eurasia and on the TP (e.g., Wu and Qian 2003; Wu et al. 2009; Ren et al. 2016), and the position and strength of the subtropical high in South China (e.g., Wang et al. 2013) could also influence summer rainfall anomalies in East China, but these factors are outside the scope of this work. Such factors that influence the rainfall anomalies over the YRB and their interaction are still unclear to some degree and require further study.

**Acknowledgements** The authors are indebted to Dr. Jianjun Xu (College of Ocean and Meteorology, Guangdong Ocean University, Zhanjiang, 524088, China) and Dr. Bin Chen (State Key Laboratory of Severe Weather, Chinese Academy of Meteorological Sciences, Beijing, 100081, China) for their helpful comments and advice on the manuscript. This study acknowledges the supported of China Meteorological Administration Special Public Welfare Research Fund

(GYHY201406001), National Natural Science Foundation of China (91644223), Major projects of Natural Science Foundation (91337000) and China Academy of Engineering Consulting Project (2017-XY-21).

## References

- Boos WR, Kuang ZM (2013) Sensitivity of the South Asian monsoon to elevated and non-elevated heating [J]. *Sci Rep* 3(6119):1192. <https://doi.org/10.1038/srep01192>
- Bougeault P, Lacarrère P (1989) Parameterization of orographic induced turbulence in a mesobeta scale model. *Mon Weather Rev* 117:1872–1890
- Chen F, Dudhia J (2001) Coupling and advanced land-surface hydrology model with the Penn State-NCAR MM5 modeling system. Part I: model implementation and sensitivity. *Mon Weather Rev* 129:569–585
- Chen LX, Gong Z, Wang Z et al (1965) The budget of atmospheric radiation energy (III). *Acta Meteorol Sin* 35(1):6–17
- Chen LX, Shmidt F, Li W (2003) Characterization of the atmospheric heat source and moisture sink over the Qinghai-Tibetan Plateau during the second TIPEX of summer 1998 and their impact on surrounding monsoon. *Meteorol Atmos Phys* 83:1–18
- Chou MD, Suarez MJ (1999) A shortwave radiation parameterization for atmospheric studies. *NASA Tech Memo* 15(104606):40
- Ding YH (1992) Effects of the Qinghai-Xizang Tibetan Plateau on the circulation features over the plateau and its surrounding areas. *Adv Atmos Sci* 9(1):112–130
- Ding YH (2009) Rainstorm and flood. Meteorological Press, Beijing, pp 18
- Duan AM, Xiao Z (2015) Does the climate warming hiatus exist over the Tibetan Plateau? *Sci Rep* 5:13711. <https://doi.org/10.1038/srep13711>
- Fang YH, Chen KQ, Chen HS et al (2018) The remote responses of early summer cold vortex precipitation in northeastern China compared with the previous sea surface temperatures. *Atmos Res* 214:399–409
- Gao YH, Xu JW, Chen DL (2015) Evaluation of WRF mesoscale climate simulations over the Tibetan Plateau during 1979–2011. *J Clim* 28(7):2823–2841. <https://doi.org/10.1175/JCLI-D-14-00300.1>
- Grell G, Devenyi D (2002) A generalized approach to parameterizing convection combining ensemble and data assimilation techniques. *Geophys Res Lett* 29(14):31–38
- He JH, Xu HM, Zhong SS (2011) The feature of atmospheric heat source over Tibetan Plateau and its influence and possible mechanism. Meteorological Press, Beijing, p 24187
- Hong SY, Lim J (2006) The WRF Single-Moment 6-Class microphysics scheme (WSM6). *J Korean Meteorol* 42:129–151
- Huang RH, Yan BL (1987) Topography and thermal forcing in the physical function of the Asian summer monsoon in the formation and maintenance. *Acta Meteorol Sin* 45(4):394–407
- Li X (2012) Sensitivity of WRF simulated typhoon track and intensity over the Northwest Pacific Ocean to cumulus schemes. *Science China Earth Sci* 42(12):1966–1978
- Li F, Zou H, Zhou LB (2017a) Study of boundary layer parameterization schemes' applicability of WRF model over complex underlying surfaces in Southeast Tibet [J]. *Plateau Meteorol* 36(2):340–357
- Li WJ, Ren HC, Zuo JQ, Ren HL (2017b) Early summer southern China rainfall variability and its oceanic drivers. *Clim Dyn.* <https://doi.org/10.1007/s00382-017-3898-0>
- Lin HJ, Ji CX, Teng DG (2010) The comparative analysis of WRF physical parameterization scheme in typhoon track and intensity [C]. In: Proceedings of the 27th annual conference of China meteorological society, pp 1–8
- Liu X, Li WP, Wu GX (2002) Inter-annual variation of the diabatic heating over the Tibetan Plateau and the northern hemispheric circulation in summer. *Acta Meteorol Sin* 60(3):267–277
- Liu YM, Wu GX, Hong JL et al (2012) Revisiting Asian monsoon formation and change associated with Tibetan Plateau forcing: II. Change *Clim Dyn* 39(5):1183–1195
- Lu CX, Yu G, Xie GD (2005) Tibetan Plateau serves as a water tower. *IEEE Trans Geosci Remote Sens* 5:3120–3123. <https://doi.org/10.1109/TGRS.2005.1526498>
- Luo HB, Chen R (1995) The impact of the anomalous heat sources over the Eastern Tibetan Plateau on the circulation over East Asia in summer half year. *Sci Meteorol Sin* 15(4):94–102
- Maussion F, Scherer D et al (2011) WRF simulation of a precipitation event over the Tibetan Plateau, China—an assessment using remote sensing and ground observations. *Hydrol Earth Syst Sci* 15(6):1795–1817
- Mlawer EJ, Taubman SJ, Brown PD, Iacono MJ, Clough SA (1997) Radiative transfer for inhomogeneous atmospheres: RRTM—a validated correlated-k model for long wave. *J Geophys Res* 102:16663–16682. <https://doi.org/10.1029/97JD00237>
- New M, Lister D, Hulme M et al (2002) A high-resolution data set of surface climate over global land areas. *Clim Res* 21(1):1–25
- Ren HC, Li W, Ren HL, Zuo J (2016) Distinct linkage between winter Tibetan Plateau snow depth and early summer Philippine Sea anomalous anticyclone. *Atmos Sci Let* 17:223–229. <https://doi.org/10.1002/asl.646>
- Skamarock WC, Klemp JB, Dudhia J et al (2008) A description of the advanced research WRF version 3. NCAR Tech Note NCAR/TN-475 + STR. <https://doi.org/10.5065/D68S4MVH>
- Stohl A, Forster C, Frank A, Seibert P, Wotawa G (2005) Technical note: the lagrangian particle dispersion model flexpart version 6.2. *Atmos Chem Phys* 5(9):2461–2474
- Tao SY, Ding YH (1980) Observational evidence of the influence of the Qinghai-Xizang (Tibetan) Plateau on the occurrence of heavy rain and severe convective storms in China. *Bull Am Meteorol Soc* 62(1):23–30
- Tao SY, Zhang QY, Zhang SL (1998) The great floods in the Changjiang River Valley in 1998. *Clim Environ Res* 3:158–167
- Wang JZ, Yang YQ, Xu XD et al (2003) A monitoring study of the 1998 rainstorm along the Yangtze River of China using TIPEX data. *Adv Atmos Sci* 20(3):425–436
- Wang Y, Xu X, Lupo AR, Li P et al (2011) The remote effect of the Tibetan Plateau on downstream flow in early summer. *J Geophys Res* 116(D19):821. <https://doi.org/10.1029/2011JD015979>
- Wang B, Xiang B, Lee JY (2013) Subtropical high predictability establishes a promising way for monsoon and tropical storm predictions [J]. *PNAS* 110(8):2718–2722
- Wang ZQ, Duan AM, Wu GX (2014a) Time-lagged impact of spring sensible heat over the Tibetan Plateau on the summer rainfall anomaly in East China: case studies using the WRF model. *Clim Dyn* 42(11–12):2885–2898
- Wang ZQ, Duan AM, Wu GX (2014b) Impacts of boundary layer parameterization schemes and air-sea coupling on WRF simulation of the East Asian summer monsoon. *Sci China Earth Sci* 44(03):548–562
- Wang CH, Shi HX, Hu HL, Wang Y, Xi B (2015) Properties of cloud and precipitation over the Tibetan Plateau. *Adv Atmos Sci* 32(11):1504–1516. <https://doi.org/10.1007/s00376-015-4254-0>
- Wang ZQ, Duan AM, Li MS et al (2016) Influences of thermal forcing over the slope/platform of the Tibetan Plateau on Asian summer monsoon: Numerical studied with the WRF model. *Chin J Geophys* 59(5):3175–3187. [https://doi.org/10.6038/cjg20160904 \(in Chinese\)](https://doi.org/10.6038/cjg20160904)

- Wang ZQ, Duan AM, Yang S (2018) Potential regulation on the climatic effect of Tibetan Plateau heating by tropical air-sea coupling in regional models. *Clim Dyn.* <https://doi.org/10.1007/s00382-018-4218-z>
- Wu TW, Qian ZA (2003) The relation between the Tibetan winter snow and the Asian summer monsoon and rainfall: an observational investigation. *J Clim* 16:2038–2051. [https://doi.org/10.1175/1520-0442\(2003\)016%3C2038:TRBTTW%3E2.0.CO;2](https://doi.org/10.1175/1520-0442(2003)016%3C2038:TRBTTW%3E2.0.CO;2)
- Wu GX, Zhang Y (1998) Tibetan Plateau forcing and the timing of the monsoon onset over South Asia and South China Sea. *Mon Weather Rev* 126(126):913–927
- Wu B, Yang K, Zhang R (2009) Eurasian snow cover variability and its association with summer rainfall in China. *Adv Atmos Sci* 26:31–44. <https://doi.org/10.1007/s00376-009-0031-2>
- Wu GX, Liu YM, He B et al (2012) Thermal controls on the Asian summer monsoon [J]. *Sci Rep* 2(5):404. <https://doi.org/10.1038/srep00404>
- Wu GX, Zhuo HF, Wang ZQ, Liu YM (2016) Two types of summertime heating over the Asian large-scale orography and excitation of potential-vorticity forcing Over Tibetan Plateau. *Sci China Ser D* 59(10):1996–2008
- Xu XD (2009) Influence of sensitivity area of Tibetan Plateau on disaster weather and climate in China and its monitoring. *Chin Eng Sci* 11(10):96–107
- Xu XD, Miao QJ (1998) Characteristics of the Yangtze River flood and strong signal source waveform. In: Chinese Academy of Sciences, Institute of atmospheric physics (eds) East Asian monsoon and Chinese rainstorm. Meteorological Press, Beijing, p 524
- Xu XD, Zhang XJ et al (1999) 1998 during the Meiyu period boundary “water flow characteristics and continuous torrential rain in the Yangtze River Valley. In: Zhao BL, Ding YH (eds) The research on Huaihe River Basin energy and water cycle (1). China Meteorological Press, Beijing, pp 12–29
- Xu XD, Zhou MY, Bian LG, Zhang GZ (2001) Comprehensive physical images of the dynamic and thermodynamic structures of land and gas processes in the Tibetan Plateau. *Sci China Ser D* 31(5):428–440
- Xu XD, Tao SY, Wang JZ (2002a) Qinghai Tibet plateau monsoon moisture transport “big triangle fan” influence domain characteristics and Chinese regional drought flood anomalies relationship. *Acta Meteorol Sin* 60(3):258–264
- Xu XD, Zhou MY, Chen JY et al (2002b) A comprehensive physical pattern of land-air dynamic and thermal structure on the Qinghai-Xizang Plateau. *Sci China Ser D* 45(7):577–594
- Xu XD, Shi XY, Wang YQ et al (2008a) Data analysis and numerical simulation of moisture source and transport associated with summer precipitation in the Yangtze River Valley over China. *Meteorol Atmos Phys* 100(1–4):217–231. <https://doi.org/10.1007/s00703-008-0305-8>
- Xu XD, Lu CG, Shi XY et al (2008b) World water tower: an atmospheric perspective. *Geophys Res Lett* 35(20):525–530. <https://doi.org/10.1029/2008GL035867>, 2008, 1–5
- Xu XD, Zhao TL, Lu CG, Guo Y, Chen B, Liu R, Li Y, Shi X (2014) An important mechanism sustaining the atmospheric “water tower” over the Tibetan Plateau. *Atmos Chem Phys Discuss* 14(12):18255–18275
- Xu XD, Guo XL, Zhao TL et al (2017) Are precipitation anomalies associated with aerosol variations over eastern China? *Atmos Chem Phys* 17(12):1–9
- Yanai M (1961) A detailed analysis of typhoon formation. *J Meteorol Soc Jpn* 39(4):187–214
- Yanai M, Tomita T (1998) Seasonal and interannual variability of atmospheric heat sources and moisture sinks as determined from NCEP-NCAR reanalysis. *J Clim* 11(3):463–482
- Yanai M, Li CF, Song ZS (1992) Seasonal heating of the Tibetan plateau and its effects on the evolution of the Asian Summer monsoon. *J Meteorol Soc Jpn* 79(1):419–434
- Ye D, Gao Y (1979) The meteorology of the Qinghai-Xizang (Tibetan) Plateau. Science Press, Beijing, p 278
- Zhang JQ, Li N (2007) Quantitative methods for risk assessment and management of major meteorological disasters. Beijing Normal University Press, Beijing, pp 310–311
- Zhao P, Chen LX (2001a) Climatic features of atmospheric heat source/sink over the Qinghai-Xizang Plateau in 35 years and its relation to rainfall in China. *Sci China Ser D* 44(9):858–864
- Zhao P, Chen LX (2001b) Inter-annual variability of atmospheric heat source/sink over the Qinghai-Xizang (Tibetan) Plateau and its relation to circulation. *Adv Atmos Sci* 18(1):106–116

**Publisher's Note** Springer Nature remains neutral with regard to jurisdictional claims in published maps and institutional affiliations.